Synthesis of silver doped titanium dioxide nanocomposites using tea extract from *Aspalathus linearis* and evaluation of their antibacterial effects.

By

Nokubonga Kobese

A thesis submitted in partial fulfilment of the requirements for the Degree

of Magister Scientiae in NanoScience, University of the Western Cape

Supervisor : Professor Marla I. Trindade

Co-supervisor : Professor Leslie F. Petrik

September 2018

Abstract

Despite the wide success of antimicrobial agents against waterborne pathogens, waterborne disease continues to pose a threat to both mankind and animals. A major concern is that certain bacteria have developed resistance to antimicrobial agents, as a result of their overuse. Silver (Ag) nanoparticles are widely used for antibacterial purposes such as medical dressings. However, they are highly toxic to human cells. Hence, there is a great interest in developing next generation antibacterial nanoparticles that are as effective as Ag nanoparticles for antibacterial functions, while having less toxicity to human cells. Several methods can be used to generate these antimicrobial nanoparticles, one of which is green nanotechnology. Green nanotechnology uses natural plants such as tea to synthesise nanoparticles rather than chemicals, thus reduce human and animal harm and improve sustainability of antibacterial agents.

Silver-titanium nano-composites (Ag-TiO2 NCs) were synthesised with the hydrothermal method using a tea extract from *Aspalathus linearis* (Rooibos, RB), and distilled water in the presence of nitrogen. The resulting structures were characterised with high resolution transmission electron microscopy (HRTEM), energy-dispersive spectroscopy (EDS) analysis X-Ray Diffraction (XRD) and Thermogravimetric Analysis (TGA). The antibacterial characteristics of these new NCs were evaluated against 3 bacteria: *Bacillus cereus*, *Cupriavidus metallidurans*, and *Escherichia coli*.

The optimum processing conditions to produce 6-nm spherical NPs included maintaining the temperature at 90 °C, the pH at 4.35, and using RB extract at a concentration of 2 mg/mL. The size of silver NPs was reduced in acidic conditions, agglomerated in neutral

conditions, and highly reduced in alkaline conditions. Increasing the pH decreased the particle size and narrowed the particle size distribution.

Gram-positive *B. cereus* showed slight resistance or tolerance to the Ag-TiO_2 nanocomposite compared to the gram-negative bacteria *E. coli* and *C. metallidurans*. The treatment concentration required for total inhibition of *E. coli* and *C. metallidurans* growth was 100 mg/mL. Supported silver nanoparticles has shown to be a suitable way to obtain highly dispersed silver over higher surface area. This approach allowed Ag-TiO2 nanocomposite to be an efficient bactericide, with less silver amount employed.

Keywords: safe drinking water; waterborne diseases; water disinfection; antimicrobial agent; nanotechnology; nanoparticles; silver doped titanium dioxide nanocomposites; reducing agents.

Declaration

I declare that *Green synthesis of silver doped titanium nanocomposites and investigation of its antimicrobial activity*, is my own work, that it has not been submitted for any degree or examination in any other university, and that all the sources I have used or quoted have been indicated and acknowledged by complete references.

Full name: Nokubonga Kobese Date: 2018

Signed ……

Acknowledgements

First and foremost, I would wish to give thanks God Almighty for giving me the strength, knowledge, ability and chance to undertake this research study and to uphold and complete it satisfactorily. without His blessings, this accomplishment would not have been possible. My acknowledgement would be incomplete without thanking the most important source of my strength, my family particularly my mother **Nozukile Beauty Kobese**, and friends.

I would like to express gratitude to my supervisors, **Prof. Trindade** and co-supervisor, **Prof. Petrik** for their inspiration, work and patience throughout the period of the study.

I notably accord my thanks to **Dr. Missengue**, **Dr Van Zyl**, **Mr. Badmus** and Dr **Tendwa** for their prestigious mentorship, training, support and inspiration.

I appreciate the assistance of the subsequent institutions: University of the Western Cape (UWC), UWC & UCT-electron microscope unit, Cape Peninsula University- oxidation stress Department, Department of Chemistry, Environmental and Nano Science (ENS) research group, Institute for microbial Biotechnology and Metagenomics (IMBM) and University of Cape Town electron microscope unit for providing me with the mandatory laboratory facilities to hold out this work.

To the National Nanoscience Postgraduate Teaching and coaching Programme (NNPTTP), ENS and IMBM members, I will be able to relish the reminiscences we've created for years to return.

To the NNPTTP and the Department of Science and Technology who provided necessary administrative facilities and funding throughout the research work, I'm grateful.

List of abbreviations

Ag:	silver ions
$AgNO_3$:	silver nitrate
AgNPs:	silver nanoparticles
Ag-TiO_2:	silver doped titanium dioxide nanocomposite
AOP:	advanced oxidation process
Au:	Gold
Bacillus spp:	Bacillus species
COD:	chemical oxygen demand
CPG:	Casamino acid-Peptone-Glucose
Cr:	Chromium
DAEC:	diffusely adherent *Escherichia coli*
DH_2O:	distilled water
DPPH:	2,2-diphenyl-1-picrylhydrazyl
DSMZ:	Deutsche Sammlung von Mikroorganismen and Zellkulturen
E. coli:	*Escherichia coli*
EAEC:	enteroaggregative *Escherichia coli*
EDS:	Energy Dispersive X-ray Spectroscopy
EHEC:	enterohaemorrhagic *Escherichia coli*
EIEC:	enteroinvasive *Escherichia coli*
EPEC:	enteropathogenic *Escherichia coli*
ETEC:	enterotoxigenic *Escherichia coli*
Fe:	iron
FO:	forward osmosis
FRAP:	Ferric Reducing Antioxidant Power
HRTEM:	High-Resolution Transmission Electron Microscopy
HUS:	haemolytic uraemic syndrome
LB:	Lubia Bertani
MF:	microfiltration
NFs:	nanofilm
Nm:	nano meters
NMs:	Nanomaterials

NPs:	Nanoparticles
NWs:	Nanowires
OD:	Optical Density
Pd:	Palladium
Pt:	Platinum
RB:	Rooibos
Rh:	Rhodium
RO:	reverse osmosis
ROS:	reactive oxygen species
TGA:	Thermogravimetric Analysis
TiO_2:	Titanium dioxide
TPTZ:	2, 4, 6-tripyridyl-s-triazine
UF:	ultrafiltration
UN:	United Union
UN-MDGs:	United Nations Millennium Development Goals
UV :	Ultraviolet
XRD :	X-Ray Diffraction

List of figures

List of tables

Contents

Chapter 1: Literature review

1.1 Introduction

Water is a crucial natural substance that is important to the world's health, environment, and economy (Bhattacharya et al. 2013). Reliable and continued access to clean and safe water is one of the essential needs of humans (Berekaa 2016). According to a United Nations (UN 2013) report, approximately 2 billion people worldwide suffer from a lack of access to clean drinking water. Other UN statistical data demonstrate that by the year 2025, 1.8 billion people will live with water shortages (Pandey et al. 2014; Alarfaj 2013; Upadhyayula et al. 2009). Currently, there are approximately 2.5 billion people in the world who do not have access to improved water facilities, most of them living in Asia, Central and South America, and Africa. Adequate clean water and essential sanitation are crucial for humans and can never be exaggerated. Consequently, these needs top the list of the United Nations Millennium Development Goals (MDG). It has been contended that water shortages could hinder the accomplishment of the MDG (Das et al. 2014) and lead to terrible living conditions, poor hygiene practices, and spread of waterborne diseases (Upadhyayula et al. 2009; WHO and Unicef 2000).

The greatest risk to health comes from the contamination of water with disease-causing microorganisms such as helminths, protozoa, fungi, bacteria, rickettsiae, viruses, and prion; organic substances such as nitrates, plant material, food, and protein; as well as inorganic substances like ammonia and gases (Tyagi et al. 2012). Intestinal parasitic infections and diarrheal diseases (such as hepatitis A, cholera, and typhoid) caused by waterborne bacteria and enteric viruses are among the most waterborne diseases (Fonyuy 2014). The burden of waterborne diseases is often exacerbated by living

parasites entering water through faecal contamination and other organisms that strive in degraded water sources (Fonyuy 2014;WHO 2014).

1.2 Waterborne pathogens

Waterborne pathogens include bacterial agents, viral agents and parasitic agents, that cause waterborne illness. The most common pathogens gain entrance to the human body through contact with or ingestion of contaminated water, the consumption of contaminated food or beverages, contact with animals, faecal contamination, or person-to-person contact. Waterborne pathogens can cause intestinal parasitic infections and diarrheal diseases, such as hepatitis A, cholera, and typhoid, in humans. Waterborne diseases are the primary cause of mortality in most developing nations in sub-Saharan Africa and South Asia. These waterborne diseases kill approximately 2.2 million people each year with the majority of these victims are children under the age of 5 years (Sharma et al. 2009). The removal, deactivation, or killing of pathogenic microorganisms in water and wastewater treatment is essential, with sanitation being the most crucial step to in ensuring uncontaminated ecosystems and public health. Knowledge about the organisms involved is often inadequate, certain infectious agents may be eradicated or diminished, while new ones emerge, making the disinfection or treatment of water increasingly challenging.

1.2.1 *Bacillus*

Bacillus species are gram-positive, strictly aerobic, or facultatively anaerobic encapsulated bacilli, that have the feature of producing spores that are exceptionally

resistant to unfavourable conditions. They are classified into subgroups *Bacillus polymyxa*, *Bacillus subtilis* (including *Bacillus cereus* and *Bacillus licheniformis*), *Brevibacillus brevis*, and *Bacillus anthracis. Bacillus species* occur in a wide range of natural environments, such as soil and water, and are readily detected in most drinking water supplies via heterotrophic plate counts (HPC). They are often detected in portable water supplies, and even in supplies previously treated and disinfected by acceptable procedures. This is largely due to the resistance of spores to disinfection (Igbeneghu 2014)

Although most *Bacillus spp.* are harmless, a few are pathogenic to humans and animals, including *B. cereus*, which causes food poisoning. *B. cereus* is known to cause bacteraemia in immune-compromised patients as well as symptoms such as vomiting and diarrhoea. Disease may result from the ingestion of the organisms or toxins produced by the organisms.

1.2.2 *Escherichia coli pathogenic strains*

Escherichia coli is present in the normal intestinal flora of humans and animals, where it generally causes no harm. However, in other parts of the body, *E. coli* can cause serious disease, such as urinary tract infections, bacteraemia, and meningitis. A few enteropathogenic strains can also cause acute diarrhoea. Several classes of enteropathogenic *E. coli* have been identified based on different virulence factors, including enterohaemorrhagic *E. coli* (EHEC), enterotoxigenic *E. coli* (ETEC), enteropathogenic *E. coli* (EPEC), enteroinvasive *E. coli* (EIEC), enteroaggregative *E. coli* (EAEC), and diffusely adherent *E. coli* (DAEC). The first four are fairly

understood classes, but the pathogenicity and prevalence of EAEC and DAEC strains are less well established (O'Connor 2002; Nataro & Kaper 1998).

EHEC serotypes, such as *E. coli* O157:H7 and *E. coli* O111, cause diarrhoea that ranges from mild and non-bloody, to highly bloody and which is indistinguishable from haemorrhagic colitis. Between 2% and 7% of cases are at risk of developing the potentially fatal haemolytic uraemic syndrome (HUS), which is characterised by acute renal failure and haemolytic anaemia. Children under the age of 5 years are at the highest risk of developing HUS. The infectivity of EHEC strains is substantially higher than that of the other strains, although as few as 100 EHEC organisms are able to cause infection. Livestock such as cattle and sheep and, to a lesser extent, goats, pigs, and chickens, are a major source of EHEC strains. The strains have also been associated with raw vegetables, such as bean sprouts, and have been detected in a variety of water environments. Infection is associated with person-to-person transmission, contact with animals, food, and consumption of contaminated water (O'Connor 2002; Nataro et al. 1998).

Waterborne transmission of pathogenic *E. coli* has been well documented in the context of recreational contact with water and ingestion of contaminated drinking-water. Control measures that can be applied to manage potential risk from enteropathogenic *E. coli* include protection of raw water supplies from animal and human waste, adequate treatment, and protection of water during storage (O'Connor 2002; Nataro et al. 1998).

1.3 Removal of microbes from water

Water that has been contaminated with certain types of microorganisms can be very unsafe. Treating drinking water to improve the smell and taste and to remove disease-causing organisms has been necessary throughout human history. Various water treatment technologies, such as screening, filtration, centrifugal separation, sedimentation, coagulation, flocculation, aerobic, and anaerobic treatments, among others, are conventionally used. Other methods of water purification include distillation, crystallisation, evaporation, solvent extraction, oxidation, precipitation, ion exchange, microfiltration (MF), ultrafiltration (UF), reverse osmosis (RO), forward osmosis (FO), adsorption, electrolysis, and electrodialysis (Das et al. 2014). However, these treatment methods are often chemically, energetically, and operationally intensive, and thus tend to be used on large systems (Shannon et al. 2008). There are also environmental impacts associated with the various current water treatment technologies. Furthermore, many of the existing technologies for the removal of microbes, are expensive or inefficient, and many emerging contaminants are not easily removed. Strategies for the available treatment of microbe-contaminated water and wastewater are classified as two groups: physical (solar and ultraviolet (UV) radiation), and chemical disinfection (chlorination, chloramination, and ozonation) processes. Each of these processes involves the destruction or inactivation of microorganisms.

Table 1.1 Removal of microbial pollutants using conventional water treatment.

Water treatment processes		Advantages	Disadvantages	References
Physical processes	Solar radiation	Effective against bacteria, viruses, and protozoa Reduces diarrhoeal diseases in users Simple and low-cost use Minimal change in taste	Requires pre-treatment (filtration and flocculation) in water of higher turbidity Limited volumes can be treated at once Time required to treat water is long	(CDC 2012a) (CDC 2008; Dawney and Pearce 2012) (CDC 2012b)
	UV radiation	No harmful by-products Improves the taste, colour, and odour of waste water No danger of overdose	No residuals left behind after disinfection, hence possibility of regrowth Not effective in water that is highly turbid	(Olaolu et al. 2014)
Chemical processes	Chloramination	Improves the odour, taste, smell, and flavour of water Active for long periods	Ineffective in killing certain microbes such as *E. coli* Highly corrosive Harmful by-products (trihalomethanes) Certain microbes are resistant to chlorine	**(**Brockovih 2010; Olaolu et al. 2014)
	Ozonation	More effective inactivation of microbes Faster in activity than chlorine Removes taste and odour from water	Ineffective in killing larger microbes and cysts High cost of ozonation equipment Possibility of microbial regrowth Harmful to human health Forms electricity by-products such as bromate	(Olaolu et al. 2014)

Table 1.1 summarises studies that have revealed the difficulty in achieving complete elimination of microorganisms from a water distribution system using different technologies. As each conventional disinfection method has both advantages and disadvantages, no single method has emerged as the optimum (Pūle 2016). Untreated or improperly treated wastewater is known to contain pathogens that can cause disease outbreaks, hence the need for adequate treatment of wastewater before discharge into other water bodies.

1.4 Nanotechnology innovations

Nanoparticles are defined as small objects in the order of 1 to 100 nm. Nanomaterials (NMs) have been used either to improve the performance of conventional wastewater treatment technologies, as well as introduce new methods. Because of their nanoscale dimension, NMs possess unique size-dependent properties such as large surface area, fast dissolution, strong sorption, superparamagnetism, quantum confinement effect, and localised surface plasmon resonance among others, which have been successfully studied for application in wastewater treatment (Qu et al. 2013). Furthermore, because of its high efficiency and multifunctional process, NM-based wastewater treatment technology is also less dependent on a large instrumental setup (ibid).

Nanobiotechnology is presently one of the most dynamic and important research disciplines in contemporary material science, and different types of plant products are being used for the green synthesis of nanoparticles (NPs) (Kaur & Komal 2016). The development of various green procedures for the preparation of NPs is highly desirable

because of the health and environmental risks associated with conventional chemical and physical synthesis. green synthesis, apart from being eco-friendly is additionally cost effective (Kaur & Komal 2016; Jaya & Khushboo 2015).

A variety of NMs have displayed excellent antimicrobial activity against a broad range of microorganisms, leading to the development of novel NM-based disinfectants. Although it may take some time to understand the full potential of NMs for water disinfection, several NMs including carbon nanotubes (CNTs), fullerene, graphene, silver (Ag), titanium dioxide (TiO_2), zinc oxide (ZnO), magnesium oxide (MgO), and cerium oxide (CeO_2) have been proposed by Das et al. (2017) for the inactivation of microorganisms in various water matrices.

1.4.1 *Titanium dioxide (TiO_2)*

TiO_2 is a semi-conducting metal oxide (Nainani et al. 2012) that has three crystalline phases: anatase, rutile, and brookite (Bahadur et al. 2016). The anatase phase is known to display high photo-catalytic activity with an indirect wide band gap edge of 3 eV (Química et al. 2015; Bonetta et al. 2013; Blake et al. 1999), while the rutile phase shows a high refractive index and a direct wide band gap of 3.23 eV (Bahadur et al. 2016; Química et al. 2015). The wide band gap of TiO_2 makes it transparent and it cannot therefore be activated in visible light (Química et al. 2015), although is active in the UV region where electrons are infused into the conduction band, creating holes in the valence band (Bahadur et al. 2016; Nainani et al. 2012). TiO_2 presents an advantage over other semiconductors because of its unique properties, such as physical and chemical stability, low cost, high catalytic activity, high oxidative power, antibacterial activity, and valence bands that are situated at

high positive potentials (Bahadur et al. 2016; Zhao et al. 2010; Nainani et al. 2012; Seery et al. 2007).

TiO_2 has recently been utilised as part of advanced oxidation processes (AOPs) for the degradation of persistent organic compounds, disposal of microorganisms, and reduction of chemical oxygen demand (COD) from water bodies to allow for water reuse (Bethi et al. 2016; Araújo et al. 2015). TiO_2 has been well studied over the last 25 years as a antimicrobial material, and has been shown to inactivate harmful microorganisms in water and air (Bonetta et al. 2013; Li et al. 2008). Mechanisms of TiO_2 as an antimicrobial agent includes the formation of reactive oxygen species (ROS), lipid peroxidation, electrostatic interactions, and alkaline effects (Kaur & Komal 2016; Mohmood et al. 2013). Matsunaga et al. (1985) irradiated nano-TiO_2 photocatalysts with photons at a wavelength of 385 nm, thus enabling it to inhibit bacterial growth. A large amount of literature is available on the toxicity of TiO_2 in bacteria, mostly focusing on its photocatalytic and bacteriostatic effects under UV light radiation (Bonetta et al. 2013). In the absence of UV irradiation, nano-TiO_2 has demonstrated little or no bactericidal effect (Dunford et al. 1997; Nakagawa et al. 1997). TiO_2 is poisonous to both gram-negative and gram-positive bacteria. The gram-positive bacterium *B. subtilis* was less responsive to treatment with nano-TiO_2 particles than a pure culture of gram-negative *E. coli* in a bacteria–TiO_2 interaction system, possibly because of *B. subtilis*'s ability to form spores (Pal et al. 2007; Daughney et al. 2001). However, other studies have shown gram-positive bacteria to be more sensitive than their gram-negative counterparts to the antibacterial effects of TiO_2 (Metzler & Huang 2015). The antibacterial properties of TiO_2 in the context of water treatment have previously been investigated. Optimum TiO_2 concentrations ranging from 100 to 1,000 mg/L have been reported to completely disinfect water containing 10^5-10^6 *E.*

coli cells/mL in 30 min under illuminated conditions (Hossain et al. 2014; Nyamukamba 2012).

1.4.2 *Elements used for improving titanium dioxide (TiO_2) performance*

TiO_2 is reported to have antimicrobial activity (Bonetta et al. 2013; Li et al. 2008), but it requires UV light exposure to activate this antimicrobial effect (Bahadur et al. 2016; Nainani et al. 2012). In the absence of UV light, no significant antimicrobial activity has been shown for TiO_2 (Caratto et al. 2013; Dunford et al. 1997; Nakagawa et al. 1997). To overcome this aforementioned challenge, a study was conducted to modify the band gap of TiO_2 (Rasalingam et al. 2014). The modifying methods developed have been used to extend the absorption band towards the visible light spectrum (Bahadur et al. 2016; Seery et al. 2007), thus improving its photocatalytic activity (Bahadur et al. 2016). One of the methods that has been used to reduce the TiO_2 band gap is the deposition of noble metals on its surface (Seery et al. 2007), thus reducing recombination reactions (Nainani et al. 2012).

Research studies also suggest that noble metal-doped TiO_2 is an effective catalyst, showing enhanced performance compared to pure TiO_2 (Caratto et al. 2013; Li et al. 2008; Wolfrum et al. 2002). Different elements, such as metals (Ag, Fe, Cr, and others), non-metals (N, S, B, and others), and lower band gap semiconductors are usually added on the surface of TiO_2 to improve its photocatalytic activity (Bahadur et al. 2016; Nainani et al. 2012). The mechanism behind the efficiency of metal-doped catalysts relates to the production of trap charge from the transition metal ion in TiO_2, thus enhancing the efficiency of the catalyst (Araújo et al. 2015; Nainani et al. 2012). The metals or dopants act as electron traps,

increased light absorption into the visible light range, and enhance the surface electron excitation via plasmon resonance excited by visible light (Nainani et al. 2012). This deposition then produces traps to withdraw photoinduced electrons or holes, leading to a decrease in the electron-hole recombination rate of the photocatalytic process, and an increase in the visible light absorption ability of TiO_2 (Araújo et al. 2015).

1.4.3 *Mechanism of Ag-TiO_2 on microbes*

The antimicrobial mechanisms of these nanomaterials (NMs) may vary under different experimental conditions. One or several of the following processes are often encountered: (i) direct physical contact of NMs with microorganisms is established through adsorption onto the cell surface or penetration into the cell membrane, (ii) physical damage to the cell membrane causes leakage of intracellular materials (e.g., cytoplasmic biomolecules including proteins, nucleic acids, and others) leading to microbial cell death, and (iii) chemical disruption of cell structures and/or essential biological functions through the production of ROS or the release of toxic ions (e.g., Ag^+ and Zn^{2+}). These mechanisms seem to be critical in determining the feasibility of NM-based antimicrobial disinfectants. Higher antimicrobial activity has also been correlated with larger individual NM surface area. For instance, individually dispersed NMs are more toxic than NM aggregates (Liu et al. 2013).

The TiO_2 anatase phase photocatalytic reaction and its antibacterial impact was first reported in 1985 by Matsunaga et al. (1985) and has been used as an antibacterial strategy because of its superhydrophilicity and solid-oxidizing power (Bahadur et al. 2016). Since then studies on the biocidal activity of TiO_2 have been conducted intensively on a wide

variety of microorganisms including fungi, viruses, and numerous other types of microbes Bonetta et al. 2013; Foster et al. 2011; Evans & Sheel 2007).

Martínez-Castañón et al. (2008) and Bonetta et al. (2013) demonstrated the antibacterial activity of TiO_2 against *Lactobacillus acidophilus* (gram-positive bacteria), *Chlorella vulgaris* (green algae), *Saccharomyces cerevisiae* (yeast), *E. coli* (gram-negative bacteria), and *Bacillus megaterium* (gram-positive bacteria) using sunlight. Titnium dioxide has also been proposed as an alternative biocidal material in surface coating for food processing, air, and water treatment (Bonetta et al. 2013), although it's antibacterial and catalytic properties are exhibited only when it is irradiated with UV light. Therefore, further improvements are needed to avoid the use of potentially harmful UV light, and obtaining a bactericidal effect using visible light is of paramount importance.

Recently, modified forms of NP-sized TiO_2 have been investigated because of the photocatalytic antibacterial activity they display in the spectrum of visible light (Caratto et al. 2013). Zhang et al. (2010) evaluated the antibacterial effect of Ag-TiO_2 thin films against *E. coli* and *Staphylococcus aureus*. The films showed excellent antimicrobial performance under both UV light irradiation and in dark environments. However, long reaction times (3–24 h) were required to achieve effective antibacterial activity because of the limited contact area of the film. To increase the surface area of the Ag-coupled TiO_2, Cho et al. (2013) experimented with the use of a co-electrospinning method, finding Ag ions were easily oxidised to Ag_2O after the pyrolysis step. Cho et al. further developed an Ag/TiO_2 nanofilm (NF) using membranes that had surfaces enhanced with Ag NPs using a photoreduction method. This composite structure showed enhanced antibacterial activity compared with the previously reported film-type substrate. Cho et al. also developed a

facile two-step fabrication method to further enhance the surface area of electrospun TiO_2 NFs by subsequent hydrothermal synthesis of TiO_2 nanowires (NWs).

1.4.4 *Silver-doped titanium dioxide (TiO_2) nanocomposites*

Silver metal and silver solutions have been known as effective non-specific bactericidal agents for centuries, owing to their broad-spectrum antibacterial and antifungal activities, as well as high sterilisation rates and low toxicity towards mammalian cells (Bahadur et al. 2016; Zhao et al. 2010). More specifically, amongst the other noble metal NPs, silver NPs have attracted much attention in the last few decades because of their known ability to enhance the photocatalytic activity of semiconductors (Nainani et al. 2012). Moreover, the literature has shown silver to be one of the frequently used modifiers of TiO_2 in bacterial inactivation, water treatment, the food industry, and antibacterial-related fields (Muniandy et al. 2017; Araújo et al. 2015). This is a direct result of the chemical and physical properties of silver as a dopant loaded on to TiO_2. Furthermore, Ag is appealing on account of its high stability in the physiological environment of microbes, and their inability to develop resistance to it (Bahadur et al. 2016).

Titanium dioxide doped with silver has been shown to exhibit strong antibacterial action and improved photocatalytic activity (Bahadur et al. 2016; Liu et al. 2003). The improvement of photocatalytic activity is accredited to the ability of silver to capture electrons at Schottky barriers (the potential energy barrier for electrons formed at metal–semiconductor junctions) at each Ag-TiO_2 contact region, thus minimising the recombination of electrons and holes generated at the surface of TiO_2. Therefore, the charge separation is enhanced and additional electron transfer occurs, resulting in longer

electron–hole pair lifetimes (Nainani et al. 2012; Seery et al. 2007). In microbial inhibition, the silver NPs create highly oxidative free radicals after permeating the bacterial membrane, thereby killing the bacteria (Bahadur et al. 2016; Liu et al. 2003). Furthermore, certain noble metals such as Au, Pd, Pt, and Rh are too expensive to be used at an industrial scale, whereas silver is a more cost-effective metal, and shows similar performance as a sensitiser (Araújo et al. 2015). This has inspired many researchers to manufacture silver-doped TiO_2-coated medical devices, sanitary ware, and air conditioning filters (Seery et al. 2007).

The advantages of Ag-TiO_2 nanocomposites expand the antibacterial functions of this NM to a broader range of working conditions (Nainani et al. 2012). Doped NMs are expected to be potential candidates for antibacterial materials, since they show high chemical durability and antibacterial activity derived from the synergistic effects of their composites (Bahadur et al. 2016). Ag-modified TiO_2 photocatalysts can also be synthesised using the hydrothermal method to load TiO_2 NPs with Ag (Castro et al. 2012; Gong et al. 2012), as this is a relatively simple process. The disadvantages of using hydrothermal methods include the high equipment cost, production of slurries that are potentially corrosive, accidental explosion of high-pressure vessels, as well as the inability to monitor the growth of crystals. Various studies have synthesised Ag-TiO_2 nanocomposites using the novel, modified sol–gel method (Kedziora et al. 2012), although the limitations of this method include the high cost of the raw materials required, by-products formed with high carbon content, and the numerous steps involved requiring close monitoring. Although the methods for the preparation of metallic NPs are well-established, there is still a need for novel, facile, green synthetic systems for the preparation of bimetallic NPs with nontoxic and biocompatible matrices. There is more interest in finding methods that use plants to

produce bimetallic nanoparticles as they are gradually becoming more available for general use (Khatami et al. 2018). Natural products can also be used for the advancement of synthesis processes of NPs.

1.5 The need for green synthesis methods

Because of rapid industrialisation and urbanisation, a large amount of perilous and superfluous chemicals, gases, and other substances are entering the environment growing need to develop eco-friendly, non-poisonous, and cost-effective approaches for the preparation of silver NPs without the need for lethal chemicals and special equipment (Rao & Tang 2017).

Different chemical and physical methods have been utilised to prepare distinctive metallic NPs, however, these techniques are often costly, and not environmentally friendly (Shaik et al. 2016). The majority of studies report utilising chemical methods, which are generally tedious, complicated, require intensive work and special equipment, and make use of toxic reducing and stabilising agents (Ocsoy et al. 2017). The chemical synthesis of NPs may also encourage the presence of certain poisonous chemical species adsorbed on their surfaces, that may have harmful impacts in their application (Loo et al. 2012).

Green approaches employing different biomolecules (including deoxyribonucleic acid (DNA), enzymes, peptides, and proteins), microorganisms, and plant extracts for NP synthesis have been investigated as alternatives to chemical methods to overcome their challenges (Rao & Tang 2017; Ocsoy et al. 2017; Loo et al. 2012). Therefore, modifying the current techniques for the synthesis of NPs by applying green chemistry standards is

viewed as a positive step as it is eco-friendly, manageable, moderately reproducible, and the finished products are often more stable (Muniandy et al. 2017; Loo et al. 2012).

Furthermore, many studies have focused on the biosynthesis of Ag-NPs utilising naturally occurring reductants (such as bacterial, fungal, and plant extracts) that are usually obtained by the confinement and incubation of bacterial strains, in addition to the reduction of silver ions, and the procedures are therefore complex and time consuming (Rao & Tang 2017). In contrast with microorganism extracts, the application of plant extracts for the synthesis of Ag-NPs is gaining momentum as it is more advantageous in terms of resource accessibility, security, reaction rate and convenience, as well as feasibility of large-scale synthesis (Rao & Tang 2017; Baker et al. 2013). Among different biomolecules, plant extracts in NP synthesis present exceptional advantages: (i) plant extract production is very simple, cost-effective, and straightforward, (ii) they are highly stable in a variety of temperatures, salt concentrations, pH conditions, and contaminations, and (iii) they require no special storage conditions (Ocsoy et al. 2017). Thus, the synthesis and assembly of Ag-TiO_2 nanocomposites would benefit from the development of less toxic and environmentally friendly green synthesis procedures.

1.5.1 `*Aspalathus linearis*

Aspalathus linearis is a plant of the Fabaceae family commonly known as Rooibos (RB). *A. linearis* is a shrubby legume that reaches a height of 1.5 to 5 ft and produces yellow flowers in spring. The plant is indigenous to mountainous areas such as the Cederberg in the western parts of South Africa. RB tea is consumed either fermented or unfermented, depending on the way the leaves are processed. The green leaves are picked, bruised, and fermented to produce a red tea, hence the name rooibos “red bush” in Afrikaans. Upon fermentation, the leaf colour changes to red or rich orange (Ulicna et al. 2003; Erickson

2002; Bramati et al. 2002). Various studies have shown *A. linearis* to be a good source of phenolic compounds and antioxidants. RB contains bioactive constituents such as phenolic and flavonoid components (Salkić et al. 2014) and is believed to be a potential chemical reduction agent (Joubert et al. 1996).

The basic structure of flavonoids is the flavan nucleus, consisting of 15 carbon atoms in three rings (C6-C3-C6) (Pietta 2000). The main phenolic compounds present contain flavones, flavanones, and flavonols (Ayeleso et al. 2014; Sasi et al. 2014; Simpson et al. 2013). Aspalathin, a rare C-C dihydrochalcone glycoside with two structurally linked chalcones (nothofagin and aspalalinin), was shown to be the most bioactive compound (Joubert et al. 1996). These bioactive components are believed to play roles as potential chemical reduction agents (Joubert et al. 1996). In this study, the green synthesis of Ag-TiO_2 nanocomposites engineered for the first time via a green chemistry process using *A. linearis* leaf extract as an effective chelating agent without the use of any acid or base standard components, is described.

1.6 Proposal

1.6.1 *Problem statement*

The world is faced with a burden of emerging waterborne pathogens, which are becoming increasingly resistant to conventional disinfection methods. The use of TiO_2 NPs in water treatment shows promises because of its efficiency in the degradation of organic pollutants and inactivation of microorganisms in water. The application of TiO_2 presents several shortcomings, the major one being that its bactericidal effect is only activated under UV irradiation, with little to no activity displayed in the absence of UV light. There is therefore

an urgent need for the design and development of eco-friendly and cost-effective antibacterial NMs in the spectrum of visible light to counteract dangerous pathogens. To this end, the green synthesis of TiO_2 modified with metal ions, which can be used in the absence of UV light and presence of sunlight, forms the basis of this investigation.

1.6.2 *Aims*

The aim of this work was to synthesise Ag-TiO_2 nanocomposite particles using tea extract from *A. linearis* (Rooibos, RB) and to investigate their antimicrobial effects.

1.6.3 *Objectives*

- To prepare silver-doped titanium dioxide NPs using *A. linearis* (RB) tea extract
- To evaluate the antibacterial properties of the Ag-TiO_2 NPs using microorganisms such as gram-positive bacteria (*B. cereus),* gram-negative bacteria *(E. coli),* and heavy metal-resistant bacteria *(C. metallidurans)* as indicators

1.6.4 *Primary research questions*

- What reaction parameters (RB concentration, pH, temperature, and time) are responsible for the shape and size of Ag-NPs?
- What is the minimum concentration of Ag-TiO_2 NPs needed to exert bactericidal and bacteriostatic effects?
- Are Ag-TiO_2 nanocomposite particles more toxic than pure Ag^+ particles?

1.6.5 *Research hypothesis statement*

Metal ions in doped TiO_2 will decrease the rate of electron-hole pair (e-/H+) recombination by acting as electron traps. The lifetime of the e-/H+ pairs is thereby increased and the capacity for OH radical production is improved, with positive effects on the oxidation of pollutants. Consequently, metal doping with Ag is an attractive alternative for enhancing TiO_2 bactericidal impact, compared to TiO_2 alone.

Chapter 2: Methodology

2.1 Introduction

This chapter provides an overview of the experimental procedures that were followed to fulfill the aims and objectives of this study. Additionally, the chapter presents the motive for the choice of methods and techniques used in the study. The experimental approach followed in pursuit of the objectives of this study is described in Figure 2.1.

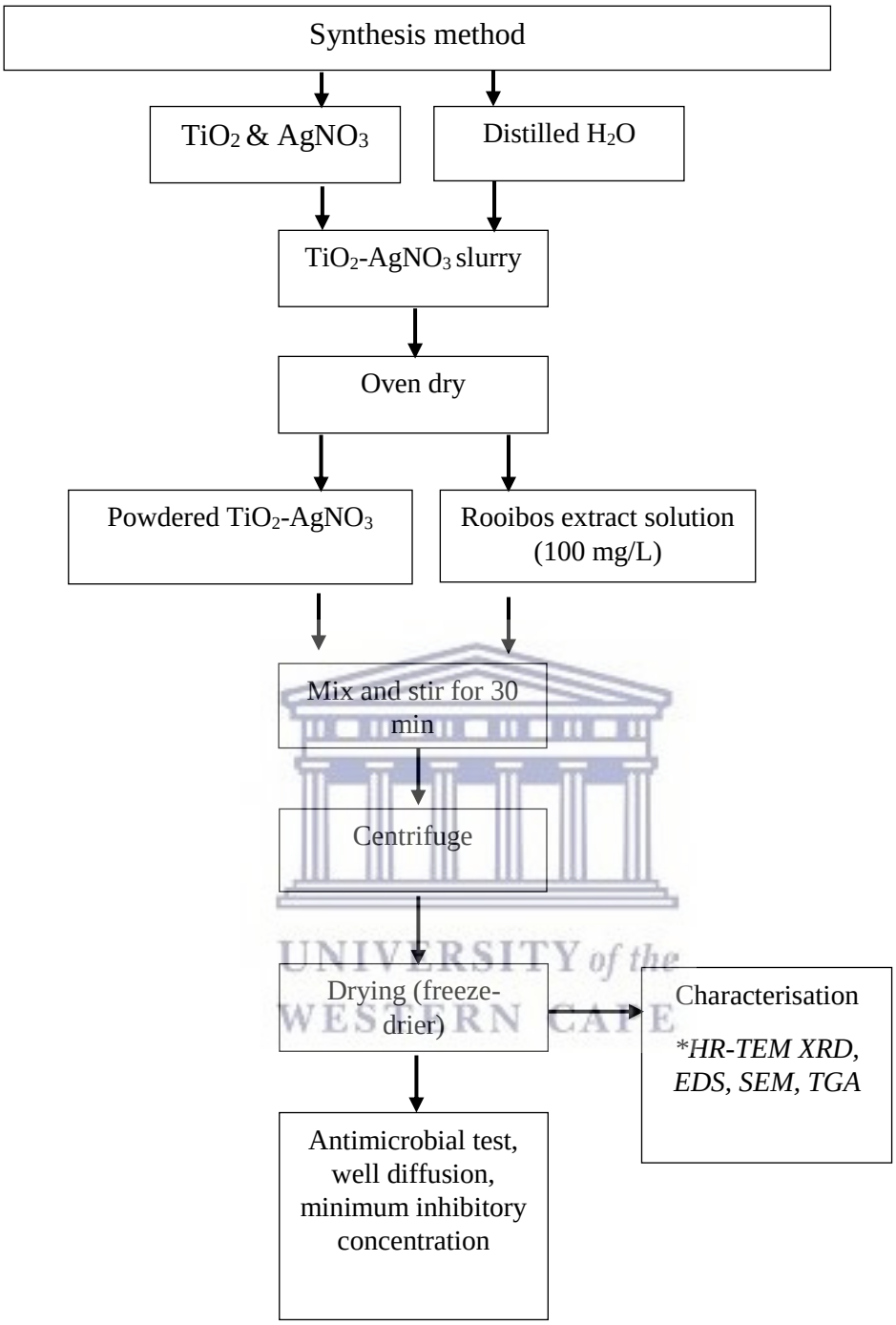

Figure 2. 1 Research protocol for the synthesis of Ag-TiO_2

*HR-TEM: high-resolution transmission electron microscopy, XRD: X-ray diffraction, EDS: energy-dispersive X-ray spectroscopy, SEM: scanning electron microscopy, TGA: thermogravimetric analysis.

2.1.1 *Research approach*

The aim of this research approach was to load silver onto TiO_2 using a green synthesis method. TiO_2 and $AgNO_3$ were suspended in distilled water (dH_2O) on a stirrer hot plate to obtain a slurry before oven-drying under high temperature to evaporate the liquid. RB extract was prepared as a stock solution and diluted with water as needed. TiO_2 and $AgNO_3$ powder was suspended in RB solution under a fume hood and mixed continuously via magnetic stirring on heat. The resultant brown precipitate solution was cooled, centrifuged, and filtered, before being washed repeatedly until the supernatant was RB-free. The product was then freeze-dried. The Ag-TiO_2 nanocomposite powder obtained was characterised using high-resolution transmission electron microscopy (HR-TEM), energy-dispersive X-ray spectroscopy (EDS), X-ray diffraction (XRD), and thermogravimetric analysis (TGA), after which antimicrobial tests were performed. All steps are described in detail in section 2.3 and shown schematically in Figure 2.1 above.

2.2 Materials

2.2.1 *Bacterial strains*

The following bacterial strains were obtained from the glycerol culture collection held at the Institute for Microbial Biotechnology and Metagenomics, University of the Western Cape (UWC), South Africa: *E. coli* DH5α, *C. metallidurans* DSMZ 2839, and *B. cereus* ATCC10702I.

2.2.2 *Chemicals*

Silver nitrate (99.80%) was purchased from Kimix Chemicals (Cape Town, SA). Tryptone powder, casein peptone (99.90%), and peptone powder (99.90%) were purchased from Merck Chemicals (Burlington, MA, USA). Yeast extract, D-(+)-glucose (99.5 %), ethanol, acetone, 2,2-diphenyl-1-picrylhydrazyl (DPPH), and tryptic soy broth were purchased from Sigma-Aldrich (St Louis, MO, USA). Casamino acid was purchased from BD (Franklin Lakes, NJ, USA). Titanium dioxide and potassium carbonate were purchased from Sigma-Aldrich (St Louis, MO, USA). Fermented and dried *A. linearis* RB tea was purchased from Coetzee & Coetzee (Pty) Ltd. (Cape Town, SA). Silver nitrate and titanium dioxide were of analytical grade and were used without further purification. The water used throughout was distilled.

2.3 Preparation of plant extracts

The polyphenol compounds were extracted from the organic fermented RB tea leaves using the method described by Saxena et al., (2014) with slight modifications. RB leaves (10 g) were extracted by soaking for 1 h in one of three different solvents: distilled water (aqueous extract), 25% ethanol, and 100% ethanol. The extraction was done at room temperature on a magnetic stirrer plate. The tea leaf solution was filtered, and the extraction process was repeated four times using the same tea leaves and a fresh solvent aliquot each time. The filtrates of each sample (RB) were mixed together and the filtered RB solution was freeze-dried.

2.4 Characterisation of *A. linearis* plant extract

The *A. linearis* freeze-dried powder obtained was characterised via antioxidant assays ferric reducing antioxidant power (FRAP) and 2,2-diphenyl-1-picrylhydrazyl (DPPH) assays, and stored in an air-tight bottle at 20 °C.

2.4.1 *2,2-diphenyl-1-picrylhydrazyl (DPPH) assay*

The DPPH assay is commonly used in natural product antioxidant studies. This assay is based on the theory that a hydrogen donor is an antioxidant, and measures compounds that are radical scavengers. The antioxidant effect is directly proportional to the disappearance of DPPH in test samples (Benzie & Strain 1996).

Monitoring DPPH via UV spectrometry has become the most commonly used method because of its simplicity and accuracy (Benzie & Strain 1996). DPPH shows a strong absorption maximum at 517 nm (purple). The colour turns from purple to yellow followed by the formation of DPPH, upon absorption of hydrogen from an antioxidant. This reaction is stoichiometric with respect to the number of hydrogen atoms absorbed. Therefore, the antioxidant effect can easily be evaluated by following the decrease of UV absorption at 517 nm.

In the experiment, 10 mg RB extract was dissolved in 100 mL methanol (1000 mg/L). Solutions of varying concentrations (500, 250, 150, 100, 50, and 0 mg/L) were prepared by diluting the prepared solution of RB1 (100% ethanol extract), RB2 (25% ethanol extract), or RB3 (distilled water extract) in methanol.

A series of ascorbic acid solutions at varying concentrations (500, 250, 150, 100, 50, and 0 mg/L) were used as references. Thereafter, 275 µL of 150 mg/L DPPH in methanol was

added to 25 µL of each prepared RB extract solution or ascorbic acid solution in a microplate. The resulting solutions were kept in the dark for 30 min. Blank solutions were prepared from 275 µL RB extract and 25 µL methanol, while the negative control comprised 275 µL DPPH and 25 µL methanol.

The absorbance of the serially diluted RB extracts, ascorbic acid, blank, and control were detected using a Biotek Power-wave XS multi-well reader. The experiments were run in triplicate and the values were converted into percentage inhibition using the formula shown in equation [1] below. The 50% inhibitory concentrations (IC_{50}) were then calculated via linear regression of the plots using Graph Pad Prism version 5.

$$\% \text{ Inhibition} = \frac{\text{Abs. Blank} - \text{Abs. Sample}) \text{ X } 100)}{(\text{Abs. Blank})} \ldots\ldots\ldots\ldots [1]$$

2.4.2 *Ferric reducing antioxidant power (FRAP) assay*

The FRAP assay is a method used to assess antioxidant power. The reduction of ferric to ferrous ion at low pH causes the formation of a coloured ferrous-tripyridyltriazine complex. FRAP values are obtained by comparing the absorbance change measured at 593 nm in test reaction mixtures with that measured in mixtures containing ferrous ions at known concentrations. This is presented as ascorbic acid equivalents (AAE) in relation to reduction activity. FRAP activity was measured according to the method developed by Benzie and Strain (1996) with slight modifications.

Briefly, acetate buffer (300 mM, pH 3.6), 10 mM 2,4,6-tripyridyl-s-triazine (TPTZ) in 0.1M HCl, and 20 mM $FeCl_3 \cdot 6H_2O$ was mixed at the ratio of 10:1:1 to obtain the working FRAP reagent. RB test samples (0.5 mL, 2 mg/mL) were mixed with 3 mL FRAP reagent. Test sample solutions were carefully prepared and agitated for 5 min on a vortex mixer

(Dragon LAB MX-S), followed by centrifugation (Eppendorf centrifuge 5810R) at 1000 rpm for a further 5 min to allow for the formation of a clear solution. Leaf extracts (100 mL) were prepared by adding 10 mg of material to 5 mL distilled water and mixing with 300 mL of the prepared FRAP reagent. The sample absorbance was measured at 593 nm with the aid of a Multiskan spectrum (Thermo Scientific, Waltham, MA, USA).

Methanol solutions of $FeSO_4 \cdot 7H_2O$ ranging from 100-2000 µM (2000, 1000, 500, 250, and 125 µM) were prepared and used for the preparation of a calibration curve of known Fe^{2+} concentration. The parameter 'equivalent concentration' was defined as the concentration of antioxidant having a ferric-TPTZ-reducing ability equivalent to that of 1 mM $FeSO_4 \cdot 7H_2O$.

2.5 Green synthesis of Ag-TiO_2 nanocomposite

The mechanism of silver-doped titanium dioxide nanocomposite synthesis involves the reduction of silver ions to zero-valent silver atoms, which then self-assemble as nanostructures (1 to 100 nm) on the surface of titanium dioxide. Silver nitrate was used as the silver precursor. The silver ions (Ag^+) were reduced by green chemistry/biosynthetic reduction using RB as the reducing and capping agent. The silver-doped titanium nanocomposite particles were synthesised using the method described in schematic diagram 2.1, which is described in further detail below.

Specific amounts of TiO_2 powder (0.42 g) and 0.005 M $AgNO_3$ salt (0.042 g) were weighed and mixed together in a 250-mL three-neck round-bottom flask. TiO_2 and $AgNO_3$ were suspended in 1 mL distilled water on a stirrer hot plate at 30 °C for 1 min at 250 rpm to obtain a slurry. The slurry was oven-dried for 2 min at 50 °C to evaporate the liquid,

thus producing a powder admixture. A stock solution of RB extract was prepared by dissolving 1 g in 10 mL, followed by the dilution of 1 mL (1000 mg/mL) stock solution in 50 mL water to obtain a tea extract solution of 2 mg/mL. The TiO_2 and $AgNO_3$ powder admixture was suspended in 50 mL RB solution (2 mg/L) under a fume hood on a continuous magnetic stirrer hot plate at 250 rpm. Reaction parameters such as the RB extract concentration ranging (0.5 and 2 mg/mL), temperature (30-90 °C), and reaction time (15-60 min), and pH (4.35-10) were individually varied to investigate the influence that these parameters may have on the size and shape of the silver-doped titanium dioxide nanocomposites. The resultant precipitate solutions were cooled, centrifuged at 4531 x *g* filtered, and washed repeatedly until the supernatant was RB-free. The nanocomposite was freeze-dried using a Telstar LoQuest dryer and the sample was first cooled to a temperature of -55 °C for 3 h. Thereafter, it was brought to a temperature of 25 °C under vacuum, following a decrease in pressure to 0.20 bar for 24 h. The Ag-TiO_2 nanocomposite was characterised via HR-TEM, high-resolution transmission electron microscopy; XRD, X-ray diffraction; EDS, energy-dispersive X-ray spectroscopy; SEM, scanning electron microscopy; and TGA, thermogravimetric analysis.

2.5.1 *Sample storage*

The silver-doped TiO_2 nanocomposite was stored in sealed polyethylene containers to avoid any moisture uptake. The bacterial glycerol stocks were stored at -80 °C. Solutions were prepared fresh and stored at 10 °C before analyses or antibacterial tests.

2.5.2 *Ag-TiO_2 synthesis through the reduction and capping of silver ions by A. linearis (Rooibos, RB)*

Silver loading on TiO_2 was carried out using RB extract as a reducing and capping agent in the presence of nitrogen gas. The various experiments are detailed in the following subsections.

2.5.2.1 Investigating the effect of reaction time

The effect of the reaction time on the silver NP size was investigated by varying the reaction time (15-60 min) used to reduce the silver ions loaded on the surface of TiO_2. Other reaction parameters such as temperature (90 °C), concentration of RB extract (2 mg/L), and pH (4.35) were kept constant. The reaction conditions and mass of TiO_2 and silver ions are summarised in Table 2.1.

Table 2. 1 Investigating the effect of the reaction time with other parameters unchanged (2 mg/L RB, pH 4.35, and 90 °C).

Sample ID	Ag (g)	TiO_2 (g)	pH	Temperature (°C)	Time (min)	Rooibos concentration (mg/mL)
AT 1	0.042	0.42	4.35	90	15	2
AT 2	0.042	0.42	4.35	90	30	2
AT 3	0.042	0.42	4.35	90	60	2

To investigate the influence of the time of reaction on the synthesis of the Ag-TiO_2 nanocomposite, samples were removed from the reaction medium at different time points between 15 and 60 min. The impact of the reaction time on the Ag-TiO_2 nanocomposite was evaluated by measuring the particle size via HR-TEM.

2.5.2.2 Investigating the effect of Rooibos (RB) extract as a reducing and stabilising agent

An efficient biosynthesis agent produces stable and small silver NPs with a narrow particle size distribution. To identify an efficient reducing and stabilising plant extract concentration, the synthesis of silver-doped TiO_2 was carried out in the presence of RB extract. The effect of the reducing and stabilising agent on silver NPs was investigated by varying the concentration of RB extract (2, 1, and 0.5 mg/mL). Other parameters including the temperature, the pH, and the optimum reaction time were kept constant. The synthesis was controlled at 90 °C and pH 4.35 for 30 min. The reaction conditions and molar mass of Ag-TiO_2 of samples AT 4, AT 5, and AT 6 are summarised in Table 2.2.

Table 2.2 Investigating the effect of the reducing and stabilising agent with other parameters unchanged (pH 4.35 at 90 °C for 30 min).

Sample ID	Ag (g)	TiO_2 (g)	pH	Temperature (°C)	Time (min)	Rooibos concentration (mg/mL)
AT 4	0.042	0.42	4.35	90	30	2
AT 5	0.042	0.42	4.35	90	30	1
AT 6	0.042	0.42	4.35	90	30	0.5

The synthesis of the Ag-TiO_2 nanocomposite was conducted as detailed in section 2.5. The effect of different concentrations of RB extract on the formation of the Ag-TiO_2 nanocomposite was evaluated systematically via HR-TEM, as described in section 2.6.

2.5.2.3 Investigating the effect of temperature

Through the following set of experiments, the effect of temperature on the Ag-TiO_2 nanocomposite particle size was investigated. Silver-doped TiO_2 nanocomposites were synthesised via green synthesis using RB extract as a reducing and stabilising agent at a pH of 4.35, with 100 mg/mL RB extract in 50 mL of distilled water, at varying temperature of 30 °C, 50 °C, 70 °C, and 90 °C for samples AT 7, AT 8, AT 9, and AT 10, respectively (Table 2.3). Other reaction parameters such as the pH, the concentration of RB extract, and the reaction time were kept constant. The reaction conditions and concentration in mg/mL of RB extract used in the synthesis are summarised in Table 2.3.

Table 2.3 Investigating the effect of temperature with other parameters unchanged (2 mg/mL RB, pH 4.35, for 30 min)

Sample ID	Ag (g)	TiO_2 (g)	pH	Temperature (°C)	Time (min)	Rooibos concentration (mg/mL)
AT 7	0.042	0.42	4.35	30	30	2
AT 8	0.042	0.42	4.35	50	30	2
AT 9	0.042	0.42	4.35	70	30	2
AT 10	0.042	0.42	4.35	90	30	2

The experiment was prepared according to the methods described in section 2.5, but the temperature was varied to 30 °C, 50 °C, 70 °C, and 90 °C, while the reaction time was 30 min and nitrogen gas was present in all cases. The samples were labelled AT 7, AT 8, AT 9, and AT 10 as shown in Table 2.1.

2.5.2.4 Investigating the effect of pH

Through this set of experiments, the influence of pH on the particle size of Ag NPs was investigated. Silver-doped TiO_2 nanocomposites were synthesised via green synthesis using RB extract as the reducing and stabilising agent at 90 °C while varying the pH level. Other reaction parameters including the temperature, concentration of RB extract, and reaction time were kept constant. The synthesis was controlled at 90 °C, using 2 mg/mL RB in 50 mL of distilled water for 30 min. An aqueous solution (50 mL) containing 2 mg/mL RB extract was adjusted to pH 7, 9, and 10 by adding a dry pinch of potassium carbonate (KOH) salt to samples AT 11, AT 12, and AT 13 respectively. The solutions were centrifuged at 4531.25 x *g*, washed several times to remove the excess RB extract, and then freeze-fried for 24 h. The reaction conditions and concentration of RB/Ag-TiO_2 used in the synthesis of samples are summarised in Table 2.4.

Table 2.4 Investigating the effect of pH with other parameters unchanged (2 mg/mL RB, at 90 °C for 30 min)

Sample ID	Ag (g)	TiO_2 (g)	pH	Temperature (°C)	Time (min)	Rooibos concentration (mg/mL)
AT 11	0.042	0.42	7	90	30	2
AT 12	0.042	0.42	9	90	30	2
AT 13	0.042	0.42	10	90	30	2

Each RB solution with varied pH level was added to a round-bottom flask containing Ag-TiO_2 powder and placed in a 90 °C oil bath for 30 min under nitrogen gas. The solutions were then centrifuged at 4531. x g and washed several times to remove the excess RB extract before freeze-drying for 24 h. The resulting samples, labelled AT 11, AT 12, and

AT 13 at pH 7, 9, and 10, respectively, were analysed via HR-TEM, XRD, EDS, SEM and TGA.

2.6 Characterisation of Ag-TiO_2 nanocomposites

This section provides a brief outline of the analytical techniques used for the characterisation of the optimised nanocomposite synthesised in this study.

2.6.1 *High-resolution transmission electron microscopy (HR-TEM)*

HR-TEM was used to analyse the size and morphology of the silver nanocrystals, to verify whether these were agglomerated or dispersed, and whether they were attached to the surface of the TiO_2, as well as to obtain images of their lattice fringes (crystallography). The HR-TEM equipment used comprised a FEI Technai20 equipped with a LaB6 emitter, operating at 200 kV and fitted with a Gatan Tridiem GIF with a 2kX2k CCD camera. The samples were prepared according to the methods described in section 2.5 and images were collected using Gatan's Digital Micrograph software. The TEM images were analysed using ImageJ software. The silver NP size distribution was plotted using origin PRO software with size data collected using imageJ, and approximately 50 particles were used to establish the histogram.

2.6.2 *Energy-dispersive X-ray spectroscopy (EDS)*

HR-TEM was coupled with an integral motorised EDS detector, which allows for the insertion and removal of samples in the TEM column for X-ray analysis. Localised EDS provides qualitative information about the elemental composition of a sample. The characteristic spectrum of X-rays emitted by the specimen after excitation by high-energy electrons is used to obtain information about the elemental composition of a sample. In this

study, EDS was used to determine the purity or quality of the silver-doped NP samples that were prepared according to section 2.5, and to determine the elemental composition.

2.6.3 *X-ray diffraction (XRD)*

XRD was utilised to study the structure of the material, including atomic arrangement, crystallite size, and atomic spacing. XRD makes use of the interaction of monochromatic X-rays with a crystalline sample. X-rays are generated in the cathode beam tube and are then separated to deliver monochromatic radiation which passes through the collimator. Bombardment of the objective specimen with the occurrent X-ray beam bar delivers a ray that is diffracted provided Braggs' law conditions are fulfilled (Chen et al. 2005).

In this study, an X-ray diffractometer XRD-D8 Bruker AXS Advance, fitted with a LynxEye indicator, with Cu $K\alpha_1$ (λ =1.5406 Å) radiation was used to determine the crystalline period of the synthesised silver-doped TiO_2 nanocomposite materials. The instrument was additionally customised via EVA and Diffraction Suite programming to identify crystallographic stages and compute the crystallite size utilising the Scherrer equation below:

$$D = \frac{0.9\lambda}{\beta cos\theta}$$

where D is the crystallite estimate, β is the full width at half maximum (FWHM) of a peak, λ is the wavelength of the X-beam radiation (0.9), θ represents Bragg's diffraction point (Chen et al. 2005). Samples were prepared according to the method described in section 2.5 and the specimens were examined in a two-theta (2θ) range scan of 5 °C to 90 ºC at room temperature. X-ray diffraction was used to investigate the mineral phase and the crystallite size of Ag-TiO_2 NPs.

2.6.4 *Thermogravimetric analysis (TGA)*

Thermo gravimetric analysis is a technique that is used to measure the variation in the mass of a sample undergoing temperature scanning in a controlled atmosphere. The sample purity and thermal stability can be determined via TGA. This technique includes the use of a sample pan that is supported on a precision balance and which is kept in a furnace and heated or cooled as required during the experiment. The weight of the sample is monitored during the experiment. A sample purge gas controls the sample environment. During analysis of a sample, the evaporation of free (unbound) water at room temperature is caused by gas flowing over the sample. This dehydration begins at room temperature and typically stops at 125 °C. Thermal decomposition can have multiple stages (weight losses) but the presence of multiple weight loss steps can also indicate the presence of multiple components in the sample.

In this study, a PerkinElmer thermogravimetric analyser (TGA7) fitted with a thermal analysis controller (TAC7/DX) was used to perform the TGA. The samples were prepared according to the method described in section 2.5 and the machine was operated under a nitrogen gas atmosphere, with samples heated from 20 °C to 600 °C at a heating rate of 5 °C/min. Approximately 3 mg of sample was weighed into the pan and analysed accordingly (Tian et al. 2016).

2.7 Investigating the antibacterial activity of silver-doped TiO_2 nanocomposites

After synthesis and characterisation of the silver-doped TiO_2 nanocomposites, assessment of the antibacterial activity of these synthesised nanomaterials was carried out. For the

purpose of this study *E. coli, B. cereus,* and *C. metallidurans* were used as indicative microorganisms to evaluate the toxicity and antibacterial activity of the Ag-TiO_2 nanocomposites.

2.7.1 *Preparation of Luria-Bertani (LB) broth and casamino acid-peptone-glucose (CPG) agar*

Luria-Bertani (LB) broth and casamino acid-peptone-glucose (CPG) agar are nutrient media commonly used for antimicrobial diffusion susceptibility testing of rapidly growing bacteria as shown in (Table 2.5; Sezonov et al. 2007). LB agar was prepared by dissolving 10 g tryptone powder, 5 g yeast extract, 10 g sodium chloride, and 15 g agar in 800 mL distilled water to a final volume of 1 L. Next, CPG agar was prepared by dissolving 1 g casamino acid, 10 g peptone powder, 5 g glucose, and 15 g agar in 800 mL distilled water to a final volume of 1 L. The prepared medium was autoclaved at 121 °C for 20 min. The medium was cooled to 51 °C, distributed into sterile petri dishes (100 mm x 15 mm) to a depth of approximately 4 mm, and allowed to solidify in a laminar flow hood. The petri dishes were left to dry for 20 min at room temperature. The prepared plates were then stored in storage bags in stacks of 10 at room temperature. Liquid media were prepared in the same way as the agar plates, without the inclusion of agar powder.

Table 2.5 Bacteria used in this study and corresponding growth media

Medium	**Bacterial strain**	**Culture temperature (°C)**
Luria-Bertani (LB) broth	*E. coli*	37
	B. cereus	37
Casamino acid-peptone-glucose (CPG)	*C. metallidurans*	28

2.7.2 *Agar diffusion antimicrobial testing*

E. coli, *B. cereus*, and *C. metallidurans* bacterial suspensions were prepared from glycerol stocks as follows: an aliquot was streaked with a sterile loop onto the respective agar medium (Table 2.5) until single colonies were observed. A single colony was picked and transferred into 5 mL of the corresponding broth in a sterile McCartney glass bottle. After overnight growth, the optical density (OD) of the bacterial culture was measured at 600 nm using a spectrophotometer, and each culture was adjusted to obtain an OD of 0.35 at 600 nm.

Initially, a 1000-µL pipette tip was used to make 8-mm wells in the agar. Thereafter, the bacterial solution was mixed using a vortex and 100 µL of the microbial culture suspension in broth was transferred to the agar surface using a pipette. Using a sterilised glass rod, the bacteria were spread uniformly over the dried surface of the agar plate and allowed to dry before loading the nanocomposite solution (100 mg/mL) into the agar wells. Separate wells were filled with 75 µL of the nanocomposite solution (RB, Ag^{+}, TiO_2, and Ag-TiO_2) or controls (distilled water). The plates were prepared according to the conditions detailed in Table 2.5 24 h prior to measuring the zone of inhibition. All antimicrobial activity tests were performed in triplicate.

2.7.3 *Liquid broth antimicrobial test of Ag-TiO_2 nanocomposites*

2.7.3.1 Preparation of nanocomposite suspensions

Ag-TiO_2 nanocomposites were suspended in distilled water (1 mL) at various concentrations (25, 50, and 100 mg/mL) for use in the antimicrobial test. After diluting the nanocomposites in distilled water, the suspension was shaken and mixed using a vortex for 30 s to fully disperse the nanocomposites.

2.7.3.2 Cell viability assessment

A 4-h acute bacterial toxicity assay was performed as follows. The inhibitory effects of aqueous suspensions of Ag-TiO_2 nanocomposites (prepared in medium) against *E. coli, B. cereus,* and *C. metallidurans* were analysed. To initiate microbial colonies for toxicity testing, one colony from each bacterial strain was transferred from the agar plates to either LB or CPG liquid growth medium and incubated overnight (LB, 37 °C; CPG, 28 °C at 11 x g). Bacterial cultures were then diluted 1:50 using fresh medium and maintained until reaching the logarithmic growth phase. The logarithmic phase was determined via spectrophotometry by measuring every 15 min to obtain a growth curve, during which several distinct growth phases were observed, including the lag phase, log phase, stationary phase, and death phase. The cells were then washed twice with liquid medium and centrifuged at 2220 x g for 10 min before resuspending in the appropriate medium. The OD of the microbial cell suspension was measured at 600 nm and adjusted to obtain a concentration of 2-3×10^7 cells/mL. For toxicity assays, solutions of Ag-TiO_2 nanocomposites (0, 25, 50, and 100 mg/L), TiO_2 (0.42 g/mL), RB extract (2 mg/mL), and LB/CPG liquid media were prepared in distilled water in 2-mL tubes. Prepared nanocomposite and control solutions (75 µL) were first pipetted into 2-mL tubes and 100 µL of microbial suspension in medium was then added and incubated at room temperature for 4 h. Thereafter, step-wise dilutions from 10^{-1} to 10^{-7} were prepared from the exposed microbial cultures, and 100 µL of each was pipetted onto LB or CPG agar plates (bacterial assays). The inoculated agar plates were incubated for 24-30 h as listed in Table 2.5, and the number of colony forming units (CFU) per mL was recorded. To ensure that the 4-h exposure of bacterial cells had no influence on the viability of the cells, CFU values for the

non-exposed controls at the beginning and at the end of the 4-h incubation period were also determined.

Control experiments were performed to investigate the bactericidal effects of the by-products from the Ag-TiO_2 nanocomposite synthesis. The amount of by-product formed in an Ag-TiO_2 nanocomposite suspension was investigated using TGA. Investigation of antibacterial effects of Ag-TiO_2 nanocomposites are further detailed in Chapter 4.

Chapter 3: Characterization of silver-doped titanium dioxide nanocomposites

3.1 Introduction

This chapter provides an overview of the characterisation and optimisation (results and discussion) of the green synthesised Ag-TiO_2 nanocomposites. The aim of this research project was to synthesise an Ag-TiO_2 nanocomposite using *A. linearis* extract, and *A. linearis* was extracted using different solvents and analysed via DPPH and FRAP techniques prior to synthesis, as RB was used in the reduction and stabilisation of the NPs. A green synthesis method was used as it is environmentally friendly and non-toxic, relatively easy and practical, and does not require any complex or expensive equipment. Furthermore, in this method the size, morphology, and distribution of the nanostructured material could be controlled.

3.2 Characterisation of *A. linearis* extract via 2,2-diphenyl-1-picrylhydrazyl (DPPH) and ferric reducing antioxidant power (FRAP) assays

This section provides a brief outline of the analytical techniques used and results obtained, followed by a discussion of RB extract characterisation. Three extraction methods (aqueous, absolute ethanol, and 25% ethanol) were used for the extraction of polyphenols from RB. The RB extraction parameters that were tested included time, concentration of the tea extract, temperature, and pH. DPPH and FRAP characterisation techniques were used to determine the best solvent to be used in the extraction of the antioxidant and phenolic constituents from RB tea. The protocol for the preparation of

the RB extract is described in section 2.3, and the DPPH and FRAP protocols are provided in sections 2.4.1 and 2.4.2, respectively.

3.2.1 *Evaluation of antioxidant activity via 2,2-diphenyl-1-picrylhydrazyl (DPPH) assay*

The DPPH assay is one of the best-known, most accurate, and frequently employed methods for evaluating antioxidant activity (Zhou et al. 2004). RB extracts were prepared according to the method described in section 2.3 prior to the evaluation of antioxidant activity via DPPH assay, using the method described in section 2.4.1. The extraction yield and antioxidant activity of plant extracts is highly dependent on the polarity of the solvent (Sineiro et al. 2008) that is used to extract the antioxidant compounds. The efficacy of three different solvents (100% ethanol, 25% ethanol in distilled water, and distilled water) to extract polyphenols from RB was investigated using the method described in section 2.3. Results from the DPPH assay are shown in Figure 3.1.

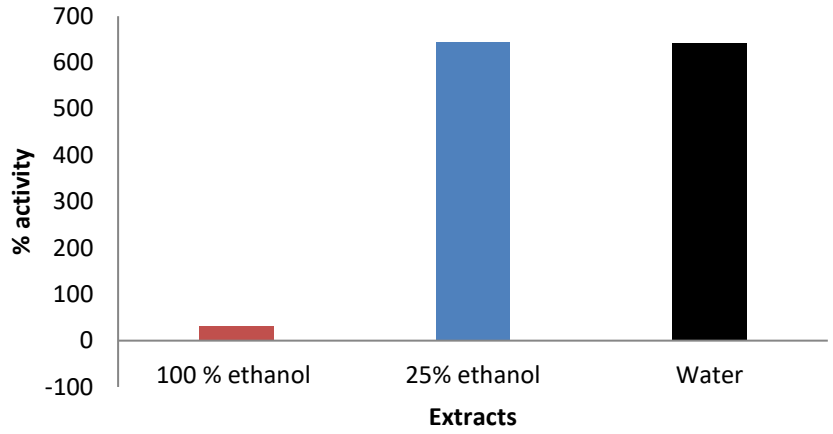

Figure 3. 1 Antioxidant activity of *Aspalathus linearis* tea extracted using three solvents (100% ethanol, 25% ethanol, and distilled water), determined via 2,2-diphenyl-1-picrylhydrazyl (DPPH) assay.

Extraction with 100% ethanol, a solvent with low polarity, showed low extraction yield and low antioxidant activity (DPPH inhibition percentage; Figure 3.1). Although the aqueous extraction of phenols from RB tea made use of a highly polar solvent, the 25% ethanol extraction method produced extracts with the highest DPPH radical-scavenging activity.

3.2.2 *Evaluation of antioxidant activity via ferric reducing antioxidant power (FRAP) assay*

The FRAP assay measures the reducing potential of an antioxidant reacting with a ferric TPTZ (Fe^{3+}-TPTZ) complex and produces a coloured ferrous tripyridyltriazine (Fe^{2+}-TPTZ; Gordon 1990). Antioxidant compounds exert reducing effects by breaking the free-radical chain through the donation a hydrogen atom. RB extracts were prepared according to the method described in section 2.3 before the evaluation of their antioxidant activity via FRAP assay using the method described in section 2.4.2. The

reducing abilities of antioxidants extracted from fermented RB extracts are shown in Figure 3.2.

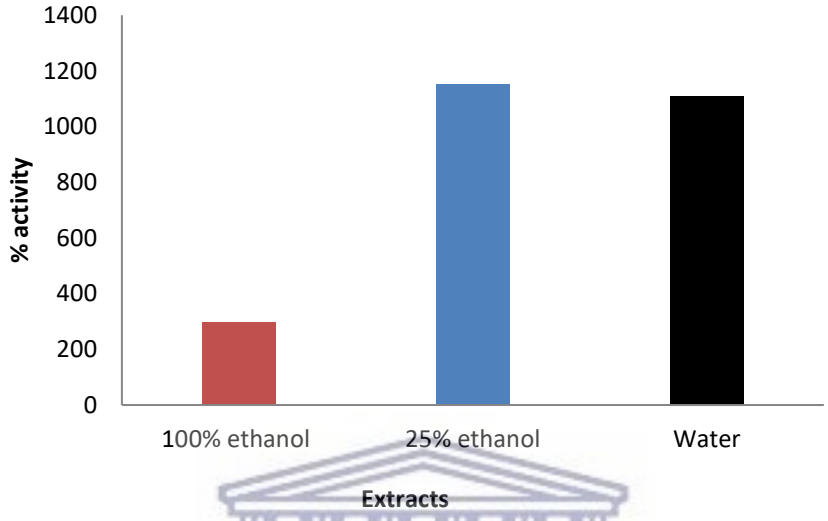

Figure 3. 2 Antioxidant activity of *Aspalathus linearis* tea extracted using three solvents (100% ethanol, 25% ethanol, and distilled water), determined via ferric reducing antioxidant power (FRAP) assay.

Results from the FRAP assay shown in Figure 3.2 confirm that the phenol extracts obtained from RB tea using 25% ethanol showed better radical scavenging activity compared to those obtained using other solvents. The best solvent for extraction was therefore 25% ethanol and this was used for RB extraction prior to the synthesis of Ag-TiO_2 nanocomposites.

3.2.3 *Summary*

In Figures 3.1 (DPPH assay) and 3.2 (FRAP assay) the main drawbacks of using the aqueous extraction solvent was the low yield of antioxidants with low polarity or liposoluble antioxidants. The 25% ethanol extraction solvent was slightly more polar

and was identified as the best extraction solvent because of its greater ability to reduce ferric ions compared to other solvents. The solubility of polyphenols depends mainly on the hydroxyl groups, molecular size, and length of the hydrocarbons (Sineiro et al. 2008). The RB extract obtained using 25% ethanol was therefore used for the synthesis of Ag-TiO_2 nanocomposites.

3.3 Optimisation of Ag-TiO_2 nanocomposite synthesis

The synthesis of small and uniform-sized NPs is challenging, and the aim of this section was therefore to optimise Ag-TiO_2 nanocomposite properties. Optimisation of the Ag-TiO_2 nanocomposites was conducted to achieve loading of 10-nm silver NPs onto TiO_2, using RB extract as the reducing and stabilising agent. The synthesis parameters that were optimised included time, temperature, extract concentration, and pH, as described in section 2.5.2, and are discussed here.

3.3.1 *The effect of reaction time on the size of Ag-TiO_2 nanoparticles (NPs)*

The quality and type of NP synthesised using green technology are greatly influenced by the length of time for which the reaction medium is incubated (Darroundi et al. 2011). Variations in the time may be revealed in several ways, such as the aggregation, shrinking, or expansion of particles after long-term storage, and their potential may be affected by their limited shelf-life (Baer et al. 2011). The optimum time for the synthesis of Ag-TiO_2 was therefore investigated by varying the synthesis time (15 min, 30 min, and 60 min for AT1, AT2, and AT3 respectively) as shown in Table 3.1. The nanocomposites were prepared according to the method described in section 2.1.1 and

all other parameters remained unchanged (90˚C, 2 mg/mL RB extract, and pH 4.35). The synthesis conditions and resulting particle sizes are listed in Table 3.1, while the particle size distribution histograms of AT1, AT2, and AT3, as well as HR-TEM images obtained using Image J, are shown in Figure 3.3.

Table 3. 1 Synthesis conditions for samples AT1, AT2, and AT3 and resultant particle size

Sample ID	Ag (g, 10% of TiO_2)	TiO_2 (g)	Temperature (°C)	Rooibos concentration (mg/mL)	Time (min)	Particle size (nm)
AT1	0.042	0.42	90	2	15	15
AT2	0.042	0.42	90	2	30	6.5
AT3	0.042	0.42	90	2	60	16

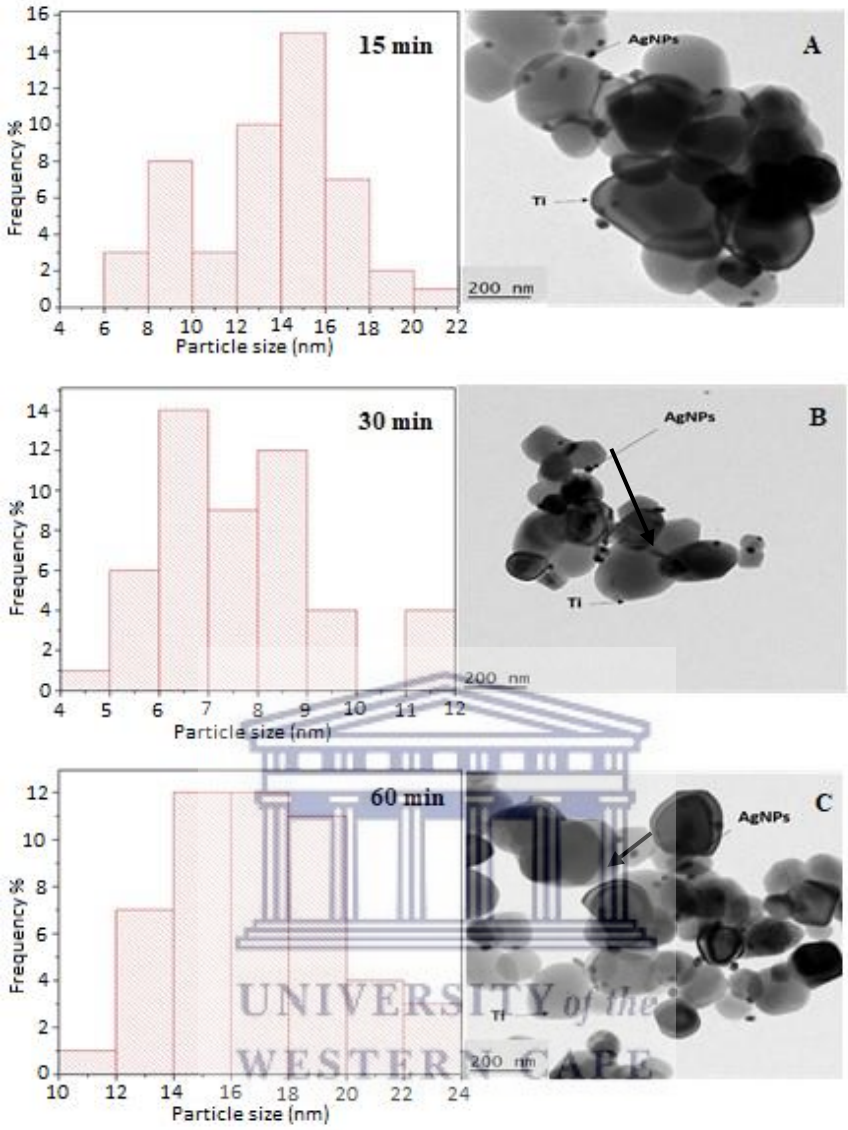

Figure 3. 3 Particle size and distribution of Ag-TiO_2, and HR-TEM images of samples showing the effect of varying the time of synthesis. A) AT1, B) AT2, and C) AT3.

The effect of time on the particle size was studied via HR-TEM. Histograms showing the particle size distribution, as well as HR-TEM images of Ag-TiO_2 synthesised over 15, 30, and 60 min using 2 mg/L RB extract are presented in Figure 3.3. The Ag-NP particle size obtained after synthesis over 15 and 60 min was 15 and 16 nm, respectively, while smaller particles (6 nm) were obtained after 30 min. We observed

that the particle size increased as the synthesis time increased to 60 min. Therefore, 30 min was identified as the optimum time required to produce particles smaller than 10 nm.

3.3.2 *The effect of Rooibos (RB) extract concentration on the size of Ag-TiO_2 nanoparticles (NPs)*

In this section, the relationship between RB extract concentration and the morphology of Ag-TiO_2 nanocomposites was investigated. The effect of the reducing agent on the silver particle size was evaluated by varying the concentration of RB extract (2 mg/L, 1 mg/L, and 0.5 mg/L for AT4, AT5, and AT6, respectively). The other reaction parameters remained unchanged (90 °C, pH 4.35, and for 30 min synthesis time). The impact of the different synthesis conditions on particle size is shown in Table 3.2, while HR-TEM images and the particle size distribution of Ag-TiO_2 nanocomposites in samples AT4, AT5, and AT6 are shown in Figure 3.4.

Table 3. 2 Synthesis conditions for samples AT4, AT5, and AT6 and resultant particle size

Sample ID	Ag (g, 10% of TiO_2)	TiO_2 (g)	Temperature (°C)	pH	Time (min)	Rooibos concentration (mg/mL)	Particle size (nm)
AT4	0.042	0.42	90	4.35	30	0.5	24-26
AT5	0.042	0.42	90	4.35	30	1	16-18
AT6	0.042	0.42	90	4.35	30	2	6-7

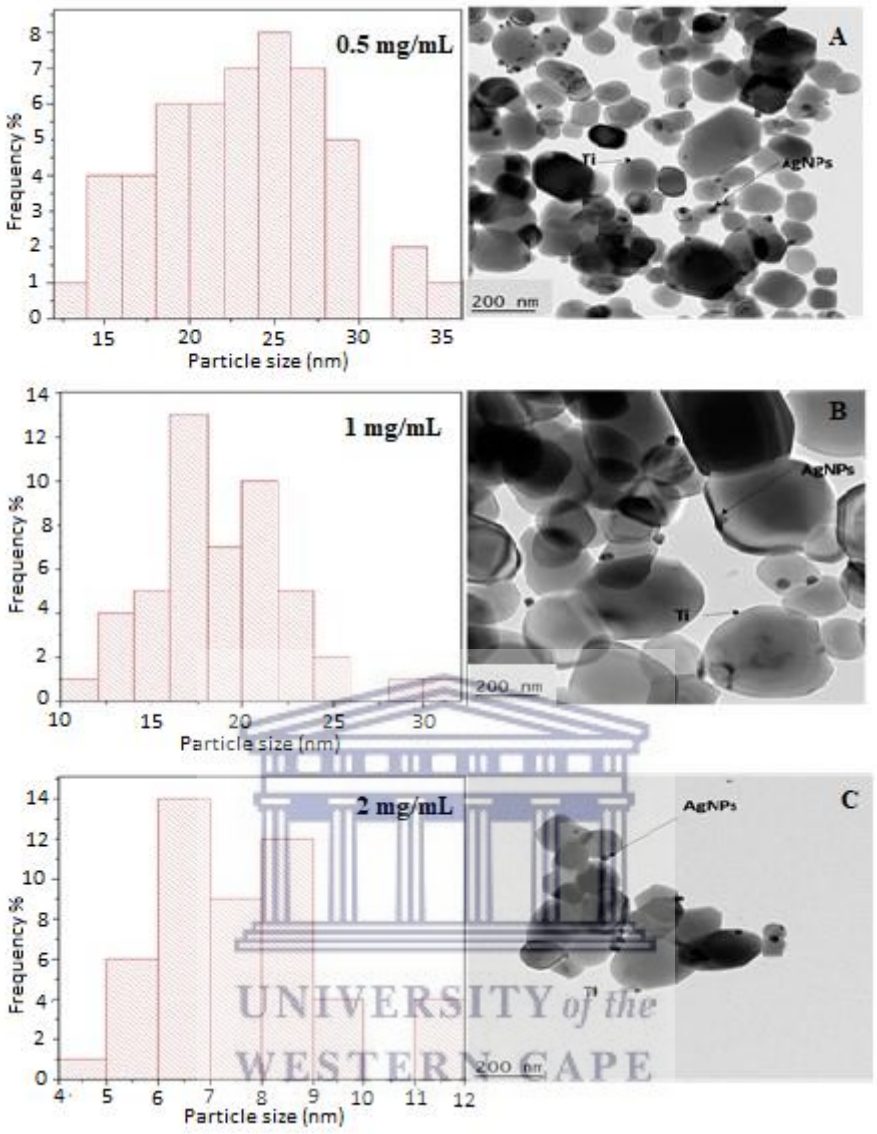

Figure 3. 4 Particle size and distribution of Ag-TiO_2, and HR-TEM images of samples showing the effect of varying the RB concentration. A) AT4, B) AT5, and C) AT6.

Various nanocomposite particle sizes were obtained by using various concentrations of RB extract during the green synthesis of Ag-TiO_2 nanocomposites. Samples AT4 (0.5 mg/L), AT 5 (1 mg/L), and AT 6 (2 mg/L) contained Ag-NPs with particle size 24-26 nm, 16-18 nm, and 6-7 nm, respectively. The size of the Ag-TiO_2 nanocomposite particle decreased as the concentration of RB increased, most likely because of the

adsorption and the stabilising effect of polyphenol antioxidants in RB. The growth mechanisms suggested by Heinlein et al. (1999) for silver NP growth imply that when the reducing agent concentration is too low, silver NPs are not sufficiently covered with the stabilising agent. Thus, coalescence of nuclei occurs due to inadequate capping of the silver ions and the sizes of the resultant particles are greater. Emmanuel et al. (2014) also reported that larger particle sizes were obtained because of the deficiency of phytochemicals to act as reducing agents. The optimal concentration of RB extract required to obtain Ag-TiO_2 nanocomposites of the desired size (5-10 nm) was 2 mg/L RB extracted using 25% ethanol. The use of RB extracts at high concentrations introduced greater concentrations of reducing and stabilising agents, which effectively reduced and capped the metal ions into metal NPs. RB extract was able to stabilise the growing nuclei by preventing potential aggregation among particles.

3.3.3 *The effect of temperature on the size of Ag-TiO_2 nanoparticles (NPs)*

Temperature is another important parameter that affects the synthesis of NPs. According to Rai et al. (2006), physical synthesis methods require very high temperatures (>350 °C), whereas chemical methods require temperatures lower than 350 °C. In most cases, the synthesis of NPs using green technology requires temperatures lower than 100 °C, and preferably ambient temperature (Rai et al. 2006).

The effect of temperature on the synthesis of silver-doped TiO_2 nanocomposite size was investigated by varying the temperature (30, 50, 70, and 90 °C in AT7, AT8, AT9, and AT10, respectively). Other reaction parameters remained unchanged (pH 4.35, 2 mg/L RB, and 30 min synthesis) as described in Table 3.3, which also shows the effects of

temperature on particle size. HR-TEM images of Ag-NP particle size distribution on TiO_2 in samples AT7, AT8, AT9, and AT10 are shown in Figure 3.5.

Table 3. 3 Synthesis conditions for samples AT7, AT8, AT9, and AT10 and resultant particle size

Sample ID	Ag (g, 10% of TiO_2)	TiO_2 (g)	pH	Time (min)	Rooibos concentration (mg/mL)	Temperature (°C)	Particle size (nm)
AT7	0.042	0.42	4.35	30	2	30	20
AT8	0.042	0.42	4.35	30	2	50	21
AT9	0.042	0.42	4.35	30	2	70	22
AT10	0.042	0.42	4.35	30	2	90	6-7

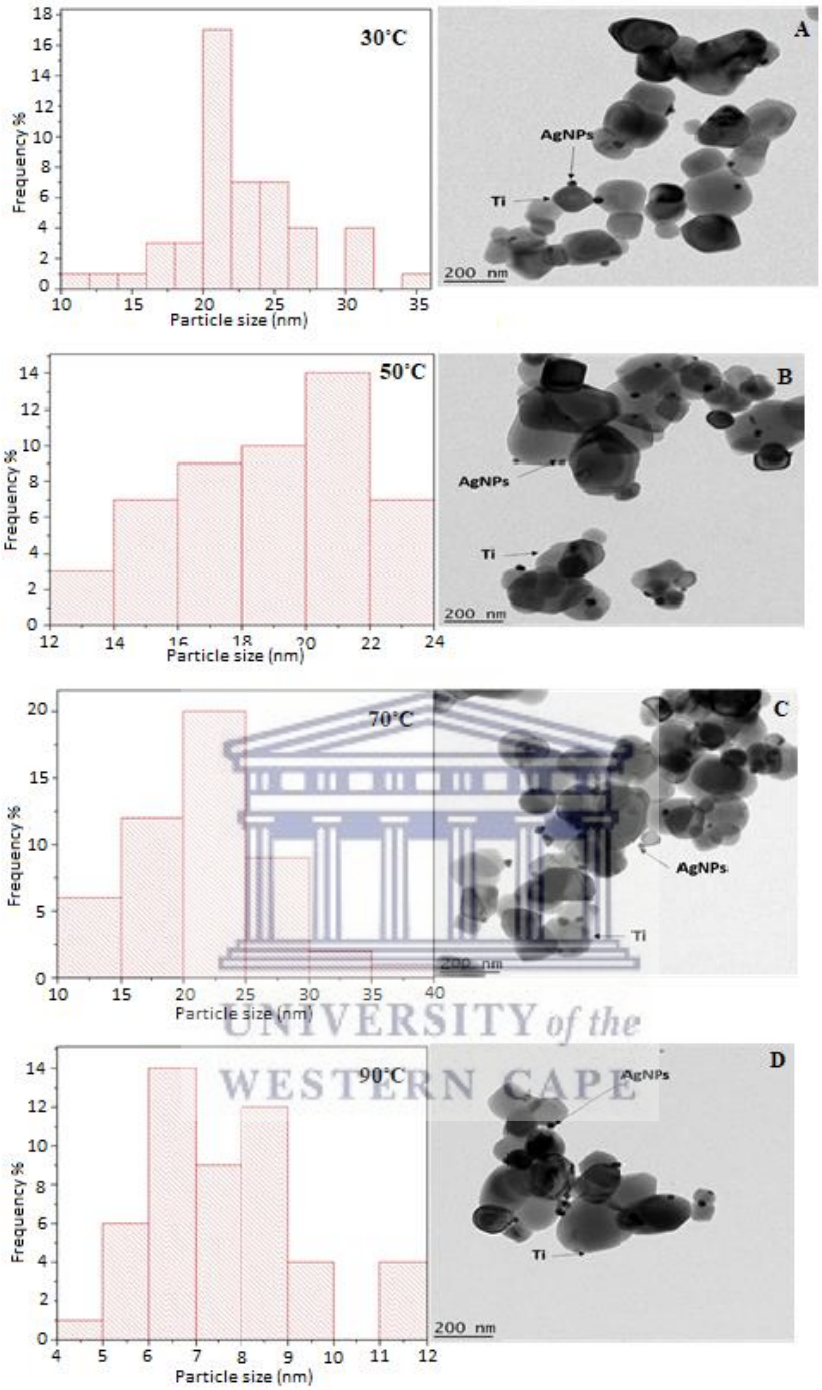

Figure 3. 5 Particle size and distribution of Ag-TiO_2, and HR-TEM images of samples showing the effect of varying the synthesis temperature. A) AT7, B) AT8, C) AT9, and D) AT10.

When the synthesis proceeded at lower reaction temperatures, the size of the NPs increased, whereas increasing the temperature resulted in smaller NPs. High temperatures are conducive to nucleation while low temperatures increase growth in the field of wet chemical NP synthesis (Khalil et al. 2014). Therefore, NPs can grow better and attain larger sizes at lower temperature, as this is conducive to growth. On the other hand, the total reaction rate is increased by increasing the reactive temperature, and high temperature is therefore conducive to nucleation. Based on the above conclusions, it was deduced that the nucleation rate constant k_1 would increase with the increasing reaction temperature, while the growth rate constant k_2 would decrease with the increasing reaction temperature.

3.3.4 *The effect pH on the size of Ag-TiO_2 nanoparticles (NPs)*

pH (potential of hydrogen) is an important factor that affects the synthesis of NPs produced by green technology methods. Researchers have discovered that the pH of the medium influences the size and texture of the synthesized NPs (Armendariz et al. 2004; Gamez et al. 2003). The effect of pH on the size of Ag-TiO_2 nanocomposites was investigated by varying the pH level to 4.36, 7.17, and 9.98 using potassium carbonate salt in samples AT11, AT12, and AT13, respectively, and evaluated via HR-TEM. Other reaction parameters remained unchanged (90 °C, 30 min, 2 mg/mL RB) as shown in Table 3.4. HR-TEM images of AT11, AT12, and AT13 and the particle size distribution of Ag-TiO_2 NPs are shown in Figure 3.6.

Table 3. 4 Synthesis conditions for samples AT11, AT12, and AT13 and resultant particle size

Sample ID	Ag (g, 10% of TiO_2)	TiO_2 (g)	Temperature (°C)	Time (min)	Rooibos concentration (mg/mL)	pH	Particle size (nm)
AT11	0.042	0.42	90	30	2	4.35	6-7
AT12	0.042	0.42	90	30	2	7.17	30-35
AT13	0.042	0.42	90	30	2	9.98	10-12

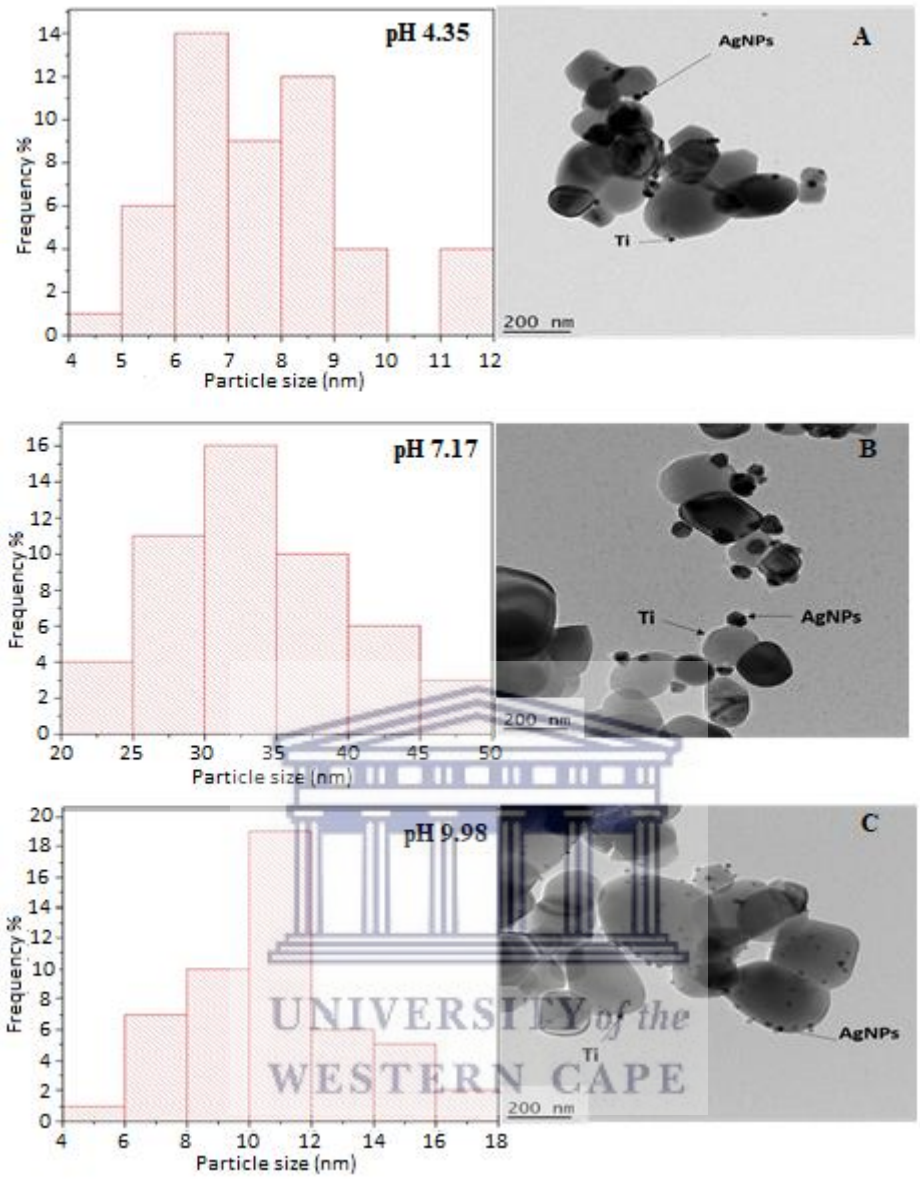

Figure 3. 6 Particle size and distribution of Ag-TiO_2, and HR-TEM images of samples showing the effect of varying the pH level. A) AT11, B) AT11, and C) AT12.

The natural pH of the nanocomposites was 4.35 (AT11) and NPs of size 6 nm were formed at this pH. At pH 7.17, larger NPs (30-35 nm) were formed, whereas at pH 9.98, intermediate-sized (10-12 nm) and highly dispersed NPs formed. The size of silver NPs was reduced in acidic condition, agglomerated in neutral conditions, and highly reduced

in alkaline conditions. Although the pH level was shown to affect the particle size, in this study the pH was not optimised further for the synthesis of NPs used for antimicrobial activity testing.

The Ag-TiO_2 nanocomposite sample AT11 was chosen as the most suitable nanocomposite for antimicrobial application in this study. This sample was appropriate because of its small particle size, which was achieved by adjusting the reaction time, temperature, and RB extract concentration, making it environmentally friendlier than other preparations. This sample was further characterised via EDS, XRD, and TGA.

3.4 Characterisation of Ag-TiO_2 using energy-dispersive X-ray spectroscopy (EDS)

In this section, the characterisation of the silver-doped TiO_2 nanocomposite sample AT11, which was chosen as the most suitable sample in section 3.4, is discussed. Sample AT11 was produced via a green hydrothermal method and the synthesis is discussed in detail in section 2.5.2. The characterisation techniques that were used to monitor the loading of the silver NPs onto TiO_2, NP morphology, and size distribution include EDS, XRD, and TGA, respectively.

3.4.1 *Energy-dispersive X-ray spectroscopy (EDS)*

Data were acquired using a JEOL JSM-6390LV SEM fitted with secondary electron detector and equipped with an attachment for EDS to enable the compositional analysis of samples. EDS was performed for the identification of elements present in the nanocomposite sample A11, produced according to the method described in section 2.5.2) and for the determination of its chemical composition. The EDS analysis of

sample AT11 in Figure 3.7 shows the presence of trace elements in the nanocomposite. Through EDS, we detected the presence of Si, C from coating, and Cu, which may have originated from the copper grid used in the HR-TEM/EDS analysis. The main elemental composition of the synthesised compounds in the silver and TiO_2 nanocomposites was also elucidated.

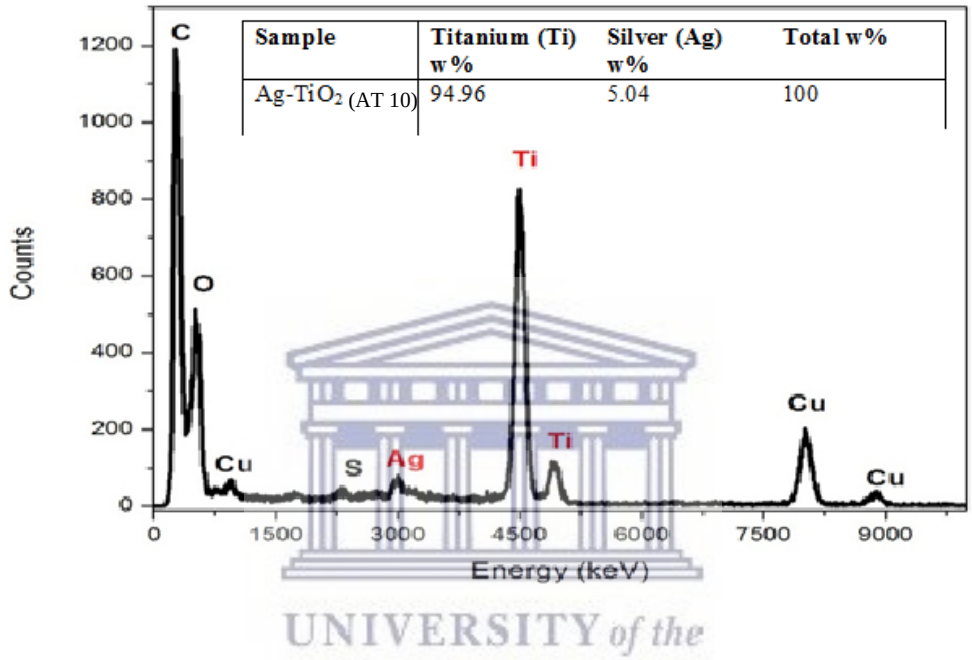

Figure 3. 7 Elemental composition of the RB extract-synthesised Ag-TiO_2 nanocomposite sample AT11 via EDS

The presence of elemental silver and titanium in the prepared Ag-TiO_2 nanocomposites was confirmed via EDS analysis as shown in Figure 3.7. The Ag content was 5.04% and Ti weight percentage was 94.96% of the doped nanocomposite. The appearance of a strong peak at approximately 4500 KeV confirmed TiO_2 as a major constituent. Low signals for the Ag-NPs formed from silver ions and C from the coating of the sample with carbon were also observed. The Cu signal arose from the Cu grid used for the analysis.

3.5 Characterisation of the Ag-TiO_2 nanocomposite via X-ray diffraction (XRD)

3.5.1 *X-ray diffraction (XRD)*

The phase composition and crystalline sizes of the synthesised Ag-TiO_2 nanocomposite sample AT11 were determined via XRD analysis (Figure 3.8). The sample was synthesised using 2 mg/L RB extract, at a pH of 3.45 and a temperature of 90 °C, for 30 min under nitrogen gas. The XRD patterns show that the sample consisted of anatase TiO_2 and silver NPs with a crystalline phase.

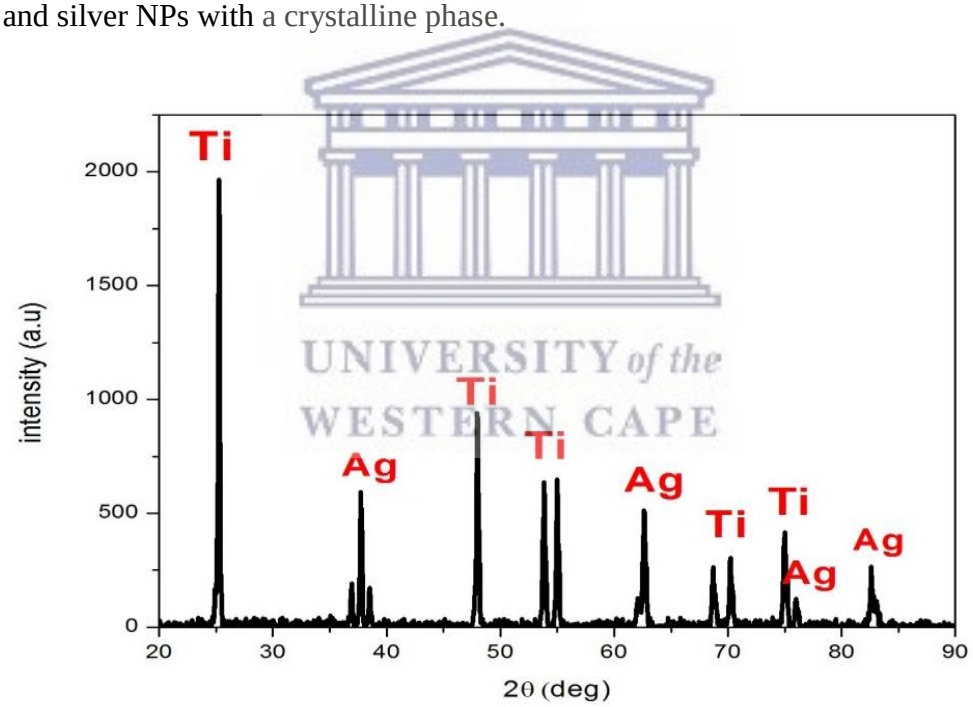

Figure 3. 8 XRD pattern of the RB extract-synthesised Ag-TiO_2 nanocomposite sample AT11

In Figure 3.8, strong diffraction peaks representing the anatase phase of TiO_2 are observed at 2θ values of 25.5°, 47.5°, 53.89°, 62.44°, 68.5°, 70.5°, 75.3°, and 84.1°. This indicates that anatase in the dominant phase in the doped titanium. The doped TiO_2

spectrum did not show any noticeable changes in the number of peaks related to the presence of the silver dopant. According to Nasr-Esfahani et al. (2008), this suggests that the Ag-NPs are well dispersed on the surface of the TiO_2.

3.6 Investigating the purity of Ag-TiO_2 via thermogravimetric analysis (TGA)

3.6.1 *Thermogravimetric analysis (TGA)*

TGA was used to investigate the thermodynamic parameters of decomposition, as well as the thermal stability of Ag-TiO_2 under nitrogen. TGA was performed at 5 °C/min, with an initial temperature of 20 °C and a final temperature of 600 °C. The TGA curves obtained for TiO_2, Ag-TiO_2 (AT11), and RB extract are shown in Figure 3.9.

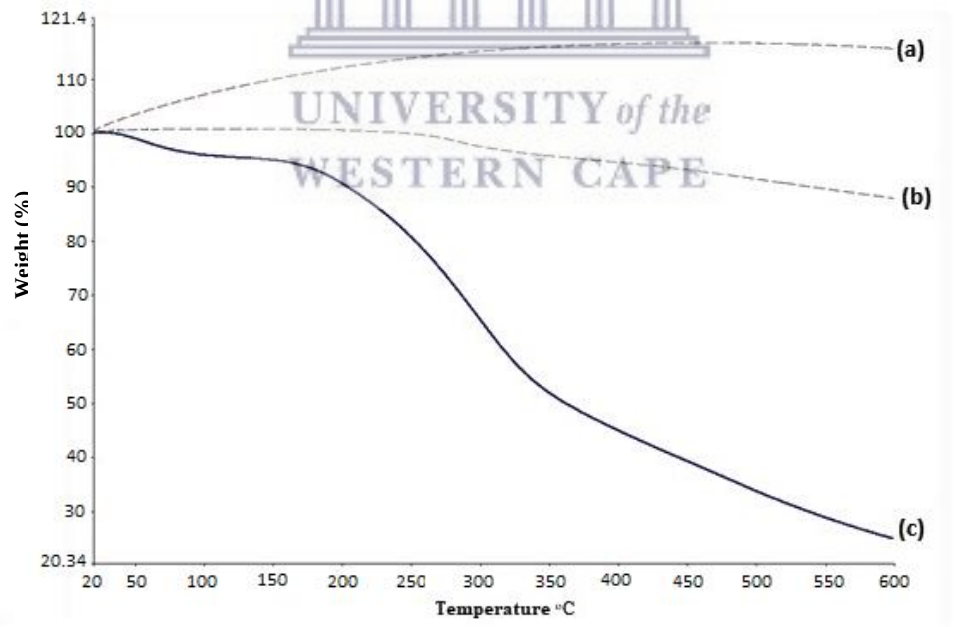

Figure 3. 9 TGA curves for A) TiO_2, B) RB extract-synthesised Ag-TiO_2 nanocomposite AT11, and C) 25% ethanolic RB extract, obtained at a heating rate of 5 ºC/min

The TGA thermogram profiles shown in Figure 3.9 represent the TGA curve of the Ag-TiO_2 nanocomposite (AT11) synthesised using 0.042 g $AgNO_3$ and 0.42 g TiO_2 analysed at a temperature of up to 600 °C in the presence of nitrogen gas. The TGA thermogram of the prepared sample (Ag-TiO_2) revealed two distinct regions of weight loss. The first degradation was attributed to the evaporation of water with a gradual weight loss of approximately 15% beginning at 25 °C and ending at 235 °C, and this loss was associated with residual water in the samples. The second step was the thermal loss of the RB capping agent that took place between 400 °C and 600 °C and was due to the slow degradation of the Ag-TiO_2 RB-stabilised nanocomposite. In this thermal degradation process, nearly 75% of the 25% ethanolic RB extract mass was lost after heating to 590 °C.

The RB extract exhibited three main stages of weight loss. The initial weight loss of 4-5% was observed at temperatures of 40 °C to 100 °C and was attributed to the decomposition of physisorbed water molecules. The second weight loss occurred in the temperature range of 160-340 °C, and this was the major thermal loss from RB due to the slow decomposition of volatile matter released from the organic RB compounds and fixed carbon content in the sample. Comparable results for TGA plant extracts were obtained by Tian et al. (2015). However, the TGA graphs for the TiO_2 powder did not exhibit any observable decomposition trends when heated to 600 °C. The total mass losses from the RB extract and the Ag-TiO_2 (AT11) sample were 75-78% and 10-12%, respectively, suggesting that Ag-TiO_2 nanocomposites are stable, which may be a result of the presence of TiO_2 in the composite. This result indicates that Ag-TiO_2 nanocomposites prepared using 25% ethanolic RB plant extracts were capped with 10% phytochemicals as compared with the weight loss observed from the RB extract. The

weight loss due to the thermal decomposition of the RB extract further allowed the determination of the quantity of the RB extract present in Ag-TiO_2 nanocomposites after the synthesis and purification of the nanocomposites.

3.6.2 *Summary*

The characterisation and optimisation of the RB extract, as well as the green synthesis of the Ag-TiO_2 nanocomposite have shown that a mixture of ethanol and water was the best solvent to use for the extraction of RB antioxidants and for the use of RB as a reducing and stabilising agent. Furthermore, several factors must be considered in the synthesis of NPs and nanocomposites and which may help to modulate particle characteristics. These include the method used for synthesis, quantity of reagents, reaction time, temperature, pH, and atmospheric air composition. Finally, optimisation is essential to obtain NPs of controlled size and morphology for potential use in environmental and biomedical applications.

The final Ag-TiO_2 nanocomposite sample AT11, which comprised smaller Ag-TiO_2 particles (6 nm), was chosen for progression to the antimicrobial study. The antimicrobial activity of this Ag-TiO_2 nanocomposite was tested against the bacteria *E. coli*, *B. cereus*, and *C. metallidurans*, and these results are presented in Chapter 4.

Chapter 4: Evaluation of the antimicrobial properties of the Ag-TiO_2 nanocomposite

4.1 Introduction

The potential of the Ag-TiO_2 nanocomposite as an antimicrobial agent was described in Chapter 1. This highlighted the need to further optimise the method of preparation of the Ag-TiO_2 nanocomposite. Here, the antimicrobial activity of the synthesised Ag-TiO_2 nanocomposite (AT11) was assessed against the gram-positive *B. cereus*, and the gram-negative *E. coli* and *C. metallidurans*. Antimicrobial activity was assessed via two different approaches: a well diffusion assay and a liquid broth dilution method.

4.2 Well diffusion assay

The antimicrobial properties of nanocomposite AT11 were assessed against the gram-positive *B. cereus* and the gram-negative *E. coli* and *C. metallidurans*, as described in section 2.7.2. Three concentrations of the Ag-TiO_2 nanocomposite (25, 50, and 100 mg/mL) and controls (0.042 g Ag, 0.42 g TiO_2, and 2 mg RB extract) were used for comparison. All antimicrobial activity tests were performed in triplicate. Treatment agents were transferred carefully to avoid spillage outside of the wells in the agar. The zones of inhibition were measured and recorded after 24 h as described in Table 4.1 and images of the well diffusion test plates are shown in Figure 4.1.

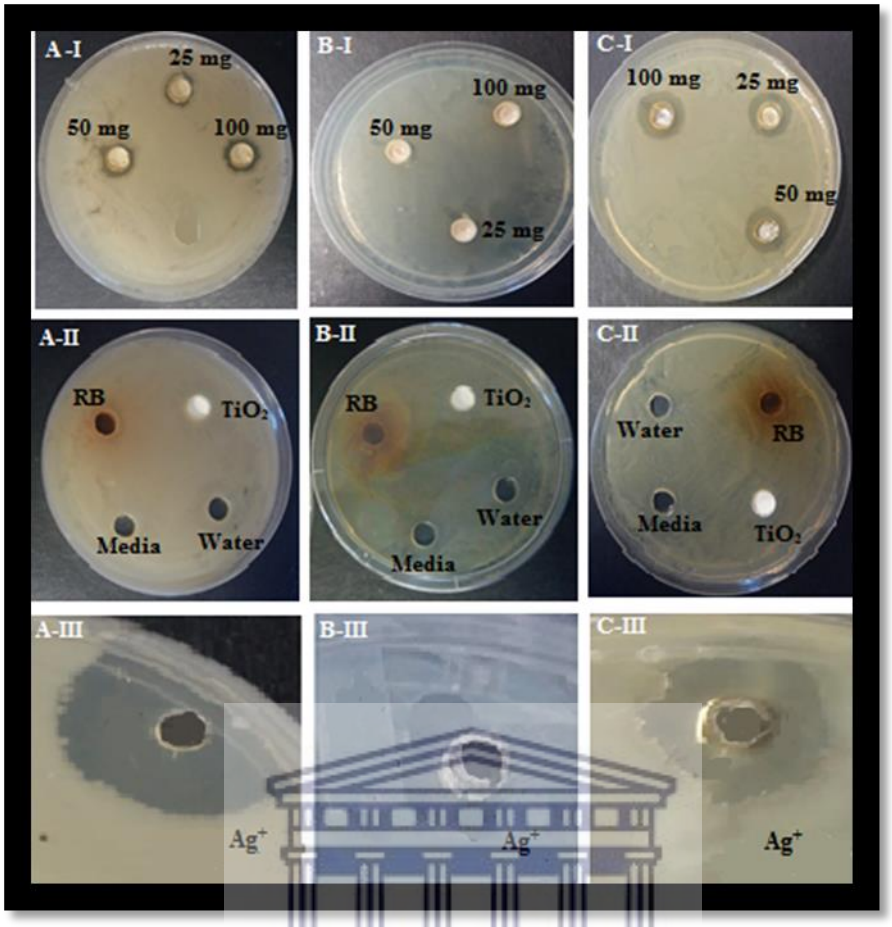

Figure 4. 1 Antimicrobial activity of the RB-synthesised Ag-TiO_2 nanocomposite AT11 (25, 50, 100 mg) and by-products (Ag, TiO_2, RB, and water) against A) I-III *B. cereus*, B) I-III *C. metallidurans*, and C) I-III *E. coli* assessed via agar well diffusion after 24 h

The highest Ag-TiO_2 nanocomposite antimicrobial activity observed was against *E. coli*, producing an inhibition zone of 8 mm, followed by that against *B. cereus* (5mm), and that against *C. metallidurans* (1 mm). A comparison between the blank and the TiO_2 sample showed that pure TiO_2 (0.42 g/mL) exhibited almost no antibacterial effect under these conditions. The growth of *B. cereus* and *E. coli* cells was inhibited by silver ions, although *C. metallidurans* bacteria survived in the presence of both silver ions and the Ag-TiO_2 nanocomposite.

Table 4. 1 Zones of inhibition measured after treatment of *B. cereus, E. coli,* and *C. metallidurans* with $AgTiO_2$ nanocomposites

Ag-TiO_2 nanocomposite concentration (mg/mL)	**Doping (%)**	**Zone of inhibition (mm)**		
		B. cereus	*C. metallidurans*	*E. coli*
25	10%	5	1	8
50	10%	5	1	8
100	10%	5	1	8

The well diffusion test showed that the Ag-TiO_2 nanocomposite exerted different antimicrobial effects on the three bacterial strains tested. There was no difference in antimicrobial activity between the different concentrations of nanocomposite used for treatment.

4.3 Broth dilution method

The extent to which the NPs diffused into agar was evaluated in the well diffusion assay. A liquid-based assay was then performed according to the method described in section 2.7. The density of the *B. cereus, C. metallidurans,* and *E. coli* microbial cell suspension in liquid media was adjusted to $2\text{-}3\times10^7$ cells/mL for use in the toxicity assays. Bacteria were inoculated in growth medium supplemented with different concentrations of Ag-TiO_2 nanocomposites (25, 50, and 100 mg/mL) and by-products (0.42 g/mL TiO_2 and 2 mg/mL RB extract). After incubation, the colony forming units (CFU) of the test organisms under all the test conditions was determined by plating dilutions on agar plates.

4.3.1 *Antimicrobial effects of by-products TiO_2 and RB extract, and Ag-TiO_2 nanocomposite on the growth of B. cereus, C. metallidurans, and E. coli*

The actual antimicrobial effects of the Ag-TiO_2 nanocomposite are listed in Table 4.2, after deducting the percentage bacterial growth inhibition caused by by-products from the percentage bacterial growth inhibition after treatment with the Ag-TiO_2 nanocomposite suspension. Dose-dependent bacterial growth inhibition was observed in all bacterial strains.

Using 100 mg/mL Ag-TiO_2, a 97% killing ratio was achieved on suspensions containing 2.8×10^7 CFU/mL *C. metallidurans* and *E. coli* in the liquid broth assay (Figure 4.2). The Ag concentration was high enough for Ag-TiO_2 to completely inhibit the growth of *C. metallidurans* at even lower concentrations (25 and 50 mg/mL), as shown in Figure 4.2 and Table 4.2. Gram-negative bacterial cell walls are more prone to mechanical breakage because of their low peptidoglycan contents (Tortora et al. 2001). *E. coli* may have been able to adapt to environment treated with Ag-TiO_2 and thus able to survive with NP exposure either by (1) modifying the peptidoglycan layer, (2) activating genes responsible for cell wall/membrane repair, or (3) ion sequestration by metabolites or proteins (Slavin et al. 2017).

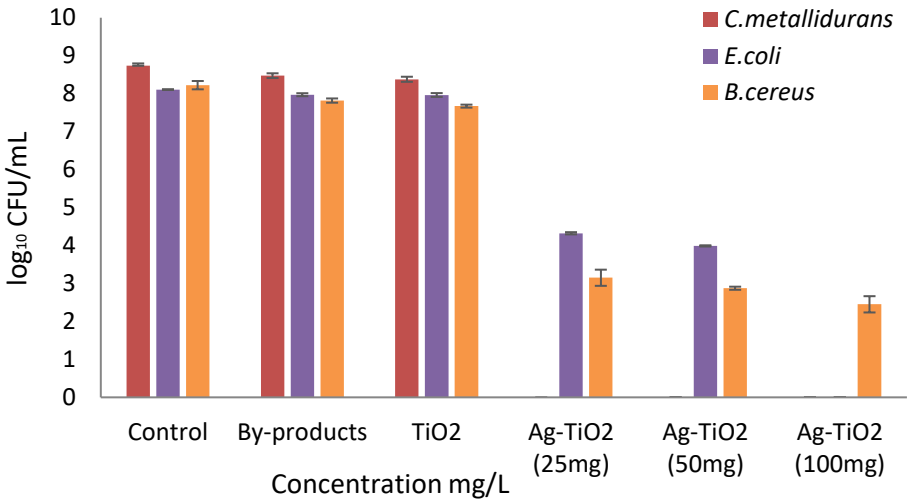

Figure 4. 2 The effect of by-products TiO_2 and RB extract, and Ag-TiO_2 nanocomposite on the growth of *B. cereus*, *C. metallidurans*, and *E. coli* treated with different concentration of Ag-TiO_2 nanocomposite (0-100 mg/mL)

Table 4. 2 Effect of Ag-TiO_2 nanocomposite on the growth of *B. cereus*, *C. metallidurans*, and *E. coli*

Bacterial strain	**Inhibitory effect of RB (%)**	**Inhibitory effect of TiO_2 (%)**	**Inhibitory effect of Ag-TiO_2 (%)**		
			25 mg/L	50 mg/L	100 mg/L
B. cereus	4.96	1.76	56.73	60.1	65.25
C. metallidurans	2.97	1.15	97.03	97.03	97.03
E. coli	1.66	0.09	45.03	49.13	98.34

B. cereus, which is resistant to a wide range of antibiotics including Ag-NPs (Sithole 2015), showed sensitivity to Ag-TiO_2 with 65.25% inhibition achieved after treating with 100 mg/mL Ag-TiO_2 nanocomposite. This is because the peptidoglycan layer of gram-positive bacteria is thicker than that of gram-negative bacteria, therefore offering greater

protection to the cell (Jung et al. 2008). Treatment with the by-products did not confer any significant antibacterial effects (Figure 4.2 and Table 4.2).

The antimicrobial activity of Ag-TiO_2 appears to be superior to that of certain pure Ag-NPs. Under similar testing conditions (e.g., using *B. cereus, C. metallidurans,* and *E. coli*), Sithole et al. (2015) reported that pure Ag-NPs (approximately 7.3 nm in size) inhibited the growth of *B. cereus, C. metallidurans,* and *E. coli* by 12.9, 65, and 61.76%, respectively, at a concentration of 50 µg/mL, making these approximately 5 times less potent than sample AT11. In this study, the Ag-TiO_2 sample showed inhibition rates of 60.1, 97.03, and 49.13 %, respectively, at a concentration of 50 µg/mL.

4.4 Discussion

The world faces a burden of emerging pathogens that are increasingly virulent and resistant to conventional disinfection methods and antibiotics (Hu et al. 2007). Doping TiO_2 with silver has been shown to confer strong antibacterial properties (Bahadur et al. 2016; Liu et al. 2003). In the present study, the green-synthesised Ag-TiO_2 nanocomposite showed potent antimicrobial activity against gram-negative and gram-positive bacteria, as shown in Figures 4.1 and 4.2. In the well diffusion assay, treatment with increasing concentrations of Ag-TiO_2 nanocomposite inoculated into LB agar wells produced similar zones of inhibition for *B. cereus* and *E. coli*. However, *C. metallidurans* cultures were not sensitive to Ag-TiO_2 nanocomposite treatment in the solid agar medium, even at the highest concentrations used. Factors that can influence the size of the zone of inhibition include the treatment concentration, the rate of diffusion of the antibacterial agents from the well into the agar, and the rate of bacterial growth. Fast-growing bacteria such as *B. cereus* and *E. coli* are more susceptible to antibiotics and NPs than slow-growing bacteria such as *C.*

metallidurans, and this may be due to the expression of stress-response genes (Mah et al. 2001; Brown et al. 1988).

In the agar diffusion method, the diffusion of antibacterial material from the well to the agar is observed through the formation of clear 'inhibition zones' without bacterial lawn. The diameter of such zones is affected by the concentration and rate of diffusion of antibacterial agents from the well into the agar (Bonev et al. 2008). As such and considering the well agar diffusion assay results (Figure 4.1), the zones of inhibition measured indicate that silver ions were more toxic than the Ag-TiO_2 nanocomposite. This could be because the silver ions were more highly concentrated than the final Ag-NPs available on the surface of TiO_2 after synthesis and several washes. Alternatively, RB polyphenols may be blocking the complete dissolution of the Ag-NPs embedded within the TiO_2 matrix, thus making the Ag-TiO_2 nanocomposite less potent than silver nitrate. As mentioned previously, the size of the zone of inhibition is affected by the concentration and rate of diffusion of the antibacterial agents from the well into the agar (Bonev et al. 2008). Therefore, lower toxicity responses obtained from the Ag-TiO_2 nanocomposite compared to that from silver ions in the well diffusion assay may be due to the delay of leaching of Ag^+ from the Ag-TiO_2 nanocomposite (oxidation of Ag-NPs from zero-valent silver to silver ions).

Although antimicrobial activities were observed in both assays (the well diffusion assay, Figure 4.1, and the liquid broth assay, Figure 4.2), better results were obtained from the liquid broth assay. Different concentrations of Ag-TiO_2 nanocomposite displayed different inhibition responses in the liquid broth assay and similar inhibition response in the well diffusion agar assay. Missengue et al. (2015) demonstrated that the antibacterial activity of nanocomposites such as silver-clinoptilolite (Ag-EHC) was not only

dependent on the concentration of Ag but also correlated with the Ag leaching rate and the size of the particles acquired after reduction. In this study, the authors showed that an increase in the amount of silver leaching out, and the amount of silver loaded, led to an increase in the microbial inhibitory zone induced by Ag-WEHC (silver ions loaded onto EHC by wet impregnation) and Ag-IEHC (silver ions loaded onto EHC by ion exchange).

However, in the current study, there may have been a delay in Ag leaching and the diffusion of the Ag-TiO_2 nanocomposite into the agar-solidified medium. This delay in Ag-TiO_2 nanocomposite contact with bacterial cells could allow the activation of a resistance mechanism to protect *B. cereus, E. coli,* and *C. metallidurans* against Ag-TiO_2 nanocomposite inhibition. However, the diffusion of the Ag-TiO_2 nanocomposite occurs more easily in liquid medium than in solid agar, and the Ag-TiO_2 nanocomposite thus inhibited the growth of all bacterial species tested in liquid medium. Furthermore, the close interaction between the suspended NPs and bacterial cells in liquid medium could allow for stronger and longer attachment and anchorage to the surface of the microbial cells, thereby causing structural changes and damage leading to cell death (Chwalibog et al. 2010).

The antibacterial activity of TiO_2 has been demonstrated in other studies. Soni et al. (2017), reported that TiO_2 possessed potent bactericidal activity against *Bacillus subtilis* and *S. aureus* as determined via agar diffusion assay. The authors reported that these antibacterial activities were proportional to the concentration of NPs. Therefore, TiO_2 might have contributed to the antibacterial activity observed in this study. Considering this, synergistic effects of a combination of antibiotics and Ag-NPs against both gram-negative and gram-positive bacteria have previously been demonstrated

(Duran et al. 2007). Ag-NPs are proposed to increase the local concentration at the site of action thus mediating bacteria cell lysis (Duran et al. 2007). Similarly, the combination of silver-doped titanium has exhibited synergistic effects against both gram-positive and gram-negative bacteria (Wong et al. 2015). Therefore, in this study, both Ag and TiO_2 NPs may have acted synergistically to demonstrate the changes seen in the liquid and solid agar assays. In agreement with this, Nigusie et al. (2018), stated that doping silver onto pure TiO_2 significantly improved the antibacterial activity of TiO_2, which was shown to be low when used in its pure state.

The antibacterial mechanism of the Ag-TiO_2 nanocomposite

The mechanism of the Ag-TiO_2 nanocomposite is thought to be mediated by the incorporation of TiO_2 NPs into an Ag matrix, which promotes Ag ion release and increases the electron donor surface energy of the coatings, leading to the enhanced antibacterial effect of the Ag-TiO_2 coatings (Chen et al. 2005). In general, the antibacterial efficacy of Ag-based coatings relies mainly on the release rate of Ag ions (Fordham et al. 2014). The antibacterial mechanism of TiO_2 includes the oxidation of all organic compounds in the microorganisms by the generated ROS, which leads to cell death (Kim et al. 2014; Motlagh et al. 2014. Ag-TiO_2 nanocomposite coatings exhibit synergistic antibacterial activity, thus making their bactericidal activities stronger than those of Ag or TiO_2 coatings (Prakash et al. 2016; Motlagh et al. 2014; Esfandiari et al. 2013; Ashkarran et al. 2011). The bactericidal capacity was also found to depend on the size characteristics of the Ag-TiO2 coatings (Esfandiari et al. 2014). However, the mechanism of the enhanced antibacterial effect of Ag-TiO_2 coatings in the absence of UV light it is still not completely understood.

The mechanism of the antibacterial functions of silver is not fully understood. Regarding Ag-NPs, it is also unclear whether their function is related to NP properties or to the release of Ag^+ ions (Hatchett & White 1996). A minimum of three mechanisms have been proposed to interpret this activity. First, Ag-NPs can attach to the bacteria cell membrane, causing structural changes or functional damages. The membrane includes mainly sulphur-containing proteins, which may be preferential sites for Ag particle attachment because of high sulphur-Ag affinity (Sondi & Salopek- Sondi 2004). This consequently causes cell death because of the increased membrane permeability and uncontrolled release of cell components (Hu et al. 2007; Amro et al. 2000).

Second, silver ions released from NPs could contribute to antibacterial activity. Silver ions are reported to cause bacterial death in several ways. Ag (I) is a strong nucleic acid binder that can form complexes with DNA and RNA (Arakawa et al. 2001). Such intercalation can lead to DNA condensation and the loss of replication ability. Respiratory enzyme activity can also be inactivated by Ag^+ binding with thiol groups in proteins (Rai et al. 2006; Feng et al. 2000). Even when loaded into composite films, Ag-NPs were still found to release silver ions into aqueous phase, which is key to the antibacterial function of such films (Sanchez-Valdes et al. 2008; Loher et al. 2008). Navarro et al. (2008) suggested that free Ag^+ ions supplied by Ag-NPs play a determinant role in Ag toxicity against *Chlamydomonas reinhardtii*, a model organism for freshwater algae.

Third, the formation of free radicals and ROS, including superoxide, hydrogen peroxide, and hydroxyl radicals, on Ag particles is responsible for their antimicrobial activities (Kim et al. 2008; KIM ET SL. 2008; Danilczuk et al. 2006). Kim et al. (2008) observed free radicals in electron spin resonance (ESR) spectra generated by Ag-NPs and related

the abolished antibacterial activity to the capture of free radicals by the antioxidant N-acetylcysteine. Choi & Hu (2008) established a connection between the ROS yield and Ag particle size and interpreted the intracellular accumulation of ROS as an important factor to the toxicity of Ag-NPs against nitrifying bacteria. The authors suggested that Ag particles smaller than 5 nm are more toxic than their larger counterparts. The Ag-NP size was controlled using RB extract in the present work, and was maintained below 7 nm, possibly indicating the possible contribution of ROS formation to Ag-mediated toxicity.

Summary

Ag-TiO_2 nanocomposite powders comprising well-dispersed Ag-NPs loaded onto the TiO_2 surface were synthesized via a hydrothermal method involving RB extract. The hydrothermal method plays an indispensable role for the control of Ag-NP size and Ag ions exist mainly in the metallic form. The superior bactericidal capability of this material is attributed to its unique structural feature of tiny Ag-NPs dispersed on the TiO_2 surface. The Ag-NP size shows great impact on the bactericidal activity. TiO_2 serves as a solid anti-aggregation support to maintain the dispersion of Ag NPs, which could also contribute to its performance. In the present study, Ag^+ ion release from suspended Ag-TiO_2 nanocomposites should not be overlooked, considering the smaller ion diffusion resistance in suspension compared to that in the well agar diffusion assay**.** A high dissolution rate is also expected because of the small particle size (Navarro et al. 2008). Improvement of the bactericidal properties is expected after fully exploiting the versatility of Ag-TiO_2 configurations.

The smaller Ag particle size may account for the higher antibacterial activity of the RB-synthesised Ag-TiO_2. This size effect has been reported by other researchers (Kim et al. 2008; Morones et al 2005). The size-dependence of antibacterial effects can be understood according to two aspects: 1) smaller particles contain more surface atoms expected to be active upon contact with bacterial cells, and 2) smaller particles have a larger fraction of atoms on low-coordination and high-energy sites (corners, edges, steps, kinks, and adatoms, among others), which makes them more active than larger particles (Zhang et al. 2010; Raimondi et al. 2005). By maintaining the Ag particle size below 7 nm, both aspects were expected to contribute to the potent antibacterial activity of Ag-TiO_2. The unique structure of the TiO_2 powder supporting highly dispersed Ag-

NPs should also account for its superior bactericidal properties. With such configuration, Ag-NPs are largely fixated on the TiO_2 surface, which minimizes their aggregation in aqueous suspensions. Unsupported Ag particles, however, tend to aggregate, which in turn reduces their effective surface area. In the RB-synthesised Ag-TiO_2 nanocomposite, TiO_2 serve as a solid anti-aggregation support to stabilise Ag dispersion. More importantly, the Ag-NPs cover a large portion of the TiO_2 surface and are exposed to the surroundings, as revealed via TEM analysis (Chapter 3). Such configuration should promote contact between Ag and the bacteria and enhance bactericidal efficacy in attacking and destroying bacterial cell membranes (Morones et al. 2005; Sondi et al. 2004). These actions were reported to increase the membrane permeability, leading to uncontrolled mass transport through the membrane, Ag penetration into cells, interaction with P- and S-containing compounds, and finally cell death (Shrivastava et al. 2007; Pal et al. 2007; Panacek et al. 2006).

Chapter 5: Conclusions

5.1 Conclusions and future aspects

In the present study, we synthesised small, uniformly dispersed silver NPs on TiO_2. Ag-TiO_2 nanocomposites were successfully synthesised via plant extract reduction of silver nitrate and TiO_2 using RB extract. The formation of Ag-TiO_2 nanocomposites was confirmed via XRD and HR-TEM coupled with EDS, and the average particle size was shown to be 6 nm. Varying the amount of RB extract showed significant effects on the particle size. The present study demonstrated that small Ag-NPs were highly dispersed over the surface of TiO_2. Increasing the pH decreased the particle size and narrowed the particle size distribution. The optimum processing conditions to produce 6-nm spherical NPs included maintaining the temperature at 90 °C, the pH at 4.35, and using RB extract at a concentration of 2 mg/mL. Next, the antibacterial activity of the Ag-TiO_2 nanocomposite against *C. metallidurans, B. cereus, and E. coli* was investigated. Gram-positive *B. cereus* showed slight resistance or tolerance to the Ag-TiO_2 nanocomposite compared to the gram-negative bacteria *E. coli* and *C. metallidurans*. The treatment concentrations required for total inhibition of *E. coli* and *C. metallidurans* growth were 100 mg/mL and 25-100 mg/mL, respectively. These results were compared with the effect of silver ions on all bacterial strains, and nanocomposite were shown to be less toxic. This opposed the literature which states that NPs are more toxic than silver ions (Morones et al. 2005). Lastly, supporting silver nanoparticles has shown to be a suitable way to obtain highly dispersed silver over higher surface area. This approach allowed Ag-TiO_2 nanocomposite to be an efficient bactericide, with only small silver amount was employed.

5.2 Recommendations for future work

This study has inspired further questions and specific work has been identified for recommendation which include:

Vary the concentration of Ag dopant to investigate whether the antimicrobial activity in gram-positive *B. cereus* can be improved.

To extract the *Aspalathus linearis* polyphenols using heat versus no heat and compare their anti-oxidation power/activity as a reducing agent.

To investigate the green synthesised Ag-TiO_2 nanocomposite photocalytic effect under solar radiation and UV radiation.

Find a method on how to calculate/ quantify the extract concentration Ag nanoparticles available after synthesis, washing and drying of the nanocomposite.

Further study on the mechanism of Ag-TiO_2 nanocomposite antimicrobial action can be done using TEM on the treated micro-organisms.

More research work can be done on Ag-TiO_2, such as to immobilize the Ag-TiO_2 nanocomposite on a membrane and test for leaching over time, as the nanocomposite content is milky and discolour water and thus cannot be used directly for water purification purposes.

Chapter 6: References

Al-Arfaj E. (2013). Structure and photocatalysis activity of silver doped titanium oxide nanotubes array for degradation of pollutants. *Superlattices and Microstructures, 62*, 285-291

Amin M.T., Alazba A.A., & Manzoor U. (2014). A Review of Removal of Pollutants from Water/Wastewater Using Different Types of Nanomaterials. *Advances in Materials Science and Engineering*, 1-24.

Amro N. A., Kotra L. P., Wadu-Mesthrige K., Bulychev, A., Mobashery S., & Liu G. (2000). High-Resolution Atomic Force Microscopy studies of the *Escherichia coli* outer membrane: Structural basis for permeability. *Langmuir, 16*(6), 2789-2796.

Arakawa H., Neault J., & Tajmir-Riahi H. (2001). Silver (I) Complexes with DNA and RNA studied by Fourier Transform Infrared Spectroscopy and Capillary Electrophoresis. *Biophysical Journal, 81*(3), 1580-1587.

Araújo B., Sônia M., Padilha P., Bozano D Castro G., Florentino A. (2015). Evaluation of pure and Ag-doped TiO_2 films in the photocatalytic activity of phenol. *Global Journal of Science Frontier Research: B Chemistry, 15*(2), 17-23.

Armendariz V., Herrera I., Peralta-videa J. R., Jose-yacaman M., Troiani H., Santiago P., & Gardea-Torresdey J. L. (2004). Size controlled gold nanoparticle formation by Avena sativa biomass: use of plants in nanobiotechnology. *Journal of Nanoparticle Research*, *6*(4), 377-382.

Ashkarran A.A., Aghigh, S.M., Kavianipour M., & Farahani, N. J. (2011). Visible light photo-and bioactivity of Ag/TiO2 nanocomposite with various silver contents. *Current Applied Physics*, *11*(4), 1048-1055.

Ayeleso A., Oguntibeju O., Aboua Y., & Brooks N. (2014). Effects of red palm oil and rooibos on sperm motility parameters in streptozotocin induced diabetic rats. *African Journal of Traditional, Complementary and Alternative Medicines*, *11*(5), 8.

Baer D. R. (2011). Surface characterization of nanoparticles: critical needs and significant challenges. *Journal of Surface Analysis*, *17*(3), 163-169.

Bahadur J., Agrawal S., Panwar V., Parveen A., & Pal K. (2016). Antibacterial properties of silver doped TiO_2 nanoparticles synthesized via sol-gel technique. *Macromolecular Research*, *24*(6), 488-493.

Baker S., Harini B., Rakshith D., & Satish S. (2013). Marine microbes: Invisible nanofactories. *Journal of Pharmacy Research*, *6*(3), 383-388.

Bartram J. (2013). Heterotrophic plate counts and drinking-water safety: The Significance of HPCs for Water Quality and Human Health. *Water Intelligence Online*, 12.

Benzie I.F., & Strain J. (1996). The Ferric Reducing Ability of Plasma (FRAP) as a measure of "Antioxidant Power": The FRAP Assay. *Analytical Biochemistry*, *239*(1), 70-76.

Berekaa M.M. (2016). Nanotechnology in wastewater treatment; influence of nanomaterials on microbial Systems. *International Journal of Current Microbiology and Applied Sciences*, *5*(1), 713-726.

Bethi B., Sonawane H., Bhanvase B., Gumfekar S. (2016). Nanomaterials based advanced oxidation processes for waste water treatment: A review. *Chemical Engineering & Processing: Process Intensification*, 109, 178-189.

Bhattacharya S., Saha I., Mukhopadhyay A., Chattopadhyay D., Ghosh U., & Chatterjee D. (2013). Role of nanotechnology in water treatment and purification*: Potential applications and implications*, *3*(3), 59–64.

Blake D., Maness P., Huang Z., Wolfrum E., Huang J., Jacoby W. (1999). Application of the photocatalytic chemistry of titanium dioxide to disinfection and the killing of cancer cells. *Separation and Purification Methods*, 28, 1–50.

Bonetta S., Motta F., Strini A., Carraro A. (2013). Photocatalytic bacterial inactivation by TiO_2 -coated surfaces. *AMB Express*, 3(1), 59

Bonev B., Hooper J., & Parisot J. (2008). Principles of assessing bacterial susceptibility to antibiotics using the agar diffusion method. *Journal of Antimicrobial Chemotherapy*, *61*(6), 1295-1301.

Bramati L., Minoggio M., Gardana C., Simonetti P., Mauri P., & Pietta P. (2002). Quantitative Characterization of Flavonoid Compounds in Rooibos Tea (Aspalathus linearis) by LC−UV/DAD. *Journal of Agricultural and Food Chemistry*, *50*(20), 5513-5519.

Brockovich E. 2010. Chloramination of drinking water. Available at: http://www.ErinBrockovichChloramination.html

Brown M.R., Allison D.G., & Gilbert P. (1988). Resistance of bacterial biofilms to antibiotics a growth-rate related effect? *Journal of Antimicrobial Chemotherapy*, *22*(6), 777-780.

Bryan J.D., & Gamelin D.R. (2005). Doped Semiconductor Nanocrystals: Synthesis, Characterization, Physical Properties, and Applications. *Progress in Inorganic Chemistry*, 47-126.

Caratto V., Aliakbarian B., Casazza A., Setti L., Bernini C., Perego P., & Ferretti M. (2013). Inactivation of Escherichia coli on anatase and rutile nanoparticles using UV and fluorescent light. *Materials Research Bulletin*, *48*(6), 2095-2101.

Castro C. A., Jurado A., Sissa D., & Giraldo S. A. (2012). Performance of Ag-TiO_2 Photocatalysts towards the Photocatalytic Disinfection of Water under Interior-Lighting and Solar-Simulated Light Irradiations. *International Journal of Photoenergy*, 1-10.

CDC. 2008. Household water treatment options in developing countries: solar disinfection. Centre for Disease Control and Prevention (CDC) Documents. Available at www.cdc.gov/../options-sodis.pdf. Accessed: 15.03.2010

CDC. 2012a. A guide to drinking water treatment and sanitation for Backcountry and travel use. Center for Disease Control and Prevention (CDC) Publication. Available at: http://www.cdc.gov/healthywater/drinking/public/water_disinf ection.htm Accessed: 15.03.2010

CDC. 2012b. Disinfection with chlorine and chloramines. Solar disinfection. Center for Disease Control and Prevention, (CDC) Publication. Available at: http://www.cdc.gov/healthywater/drinking/travel/backcountry _water_treatment.html. Accessed: 15.03.2010

Chan S.C., & Barteau M.A. (2005). Preparation of highly uniform Ag/TiO_2 and Au/TiO_2 supported nanoparticle catalysts by photodeposition. *Langmuir*, *21*(12), 5588-5595.

Chen X., Lou Y., Samia A.C.S., Burda C., Gole, J.L. (2005). Formation of oxynitride as the photocataltic enhancing site in Nitrogen-Doped Titania Nanocatalysts: Comparison to a commercial nanopowder. *Advanced Functional Materials*, 15;41-49.

Cho Y-K, Lee W.S., & Park Y.S. (2013). Significantly enhanced antibacterial activity of TiO_2 nanofibers with hierarchical nanostructures and controlled crystallinity. *The Royal Society of Chemistry*, 00, 1-3.

Choi O., & Hu Z. (2008). Size Dependent and Reactive Oxygen Species Related Nanosilver Toxicity to Nitrifying Bacteria. *Environmental Science & Technology*, *42*(12), 4583-4588.

Chwalibog C., Hotowy S., Mitura S., Sokolowska S.P. (2010). Visualization of interaction between inorganic nanoparticles and bacteria or fungi. *International Journal of Nanomedicine*, 1085.

Danilczuk M., Lund A., Sadlo J., Yamada H., and Michalik J. (2006). "Conduction electron spin resonance of small silver particles," *Spectrochimica Acta Part a-Molecular and Biomolecular Spectroscopy*, 63,189-191.

Danilczuk M., Lund A., Sadlo J., Yamada H., & Michalik J. (2006). Conduction electron spin resonance of small silver particles. *Spectrochimica Acta Part A: Molecular and Biomolecular Spectroscopy*, *63*(1), 189-191.

Darroudi M. (2011). Time-dependent effect in green synthesis of silver nanoparticles. *International Journal of Nanomedicine*, 677.

Das R. (2017). Nanohybrid Catalyst based on Carbon Nanotube. *Carbon Nanostructures*, 75-104.

Das R., Vecitis C.D., Schulze A., Cao B., Ismail A. F., Lu X., & Ramakrishna S. (2014). Recent advances in nanomaterials for water protection and monitoring. *Chemical Society Reviews*, *46*(22), 6946-7020.

Daughney C.J., Fowle D.A., & Fortin D. (2001). The effect of growth phase on proton and metal adsorption by Bacillus subtilis. *Geochimica et Cosmochimica Acta*, *65*(7), 1025-1035.

Dawney B., & Pearce J.M. (2012). Optimizing the solar water disinfection (SODIS) method by decreasing turbidity with NaCl. *Journal of Water, Sanitation and Hygiene for Development, 2*(2), 87.

Dunford R., Salinaro A., Cai L., Serpone N., Horikoshi S., Hidaka H., & Knowland J. (1997). Chemical oxidation and DNA damage catalysed by inorganic sunscreen ingredients. *FEBS Letters*, *418*(1-2), 87-90.

Emmanuel R., Karuppiah C., Chen S., Palanisamy S., Padmavathy S., & Prakash, P. (2014). Green synthesis of gold nanoparticles for trace level detection of a hazardous pollutant (nitrobenzene) causing Methemoglobinaemia. *Journal of Hazardous Materials*, 279, 117-124.

Erdem A., Metzler D., Cha D., & Huang C. P. (2014). Inhibition of bacteria by photocatalytic nano-TiO2 particles in the absence of light. *International Journal of Environmental Science and Technology*, *12*(9), 2987-2996.

Erickson L. (2003). Rooibos Tea: Research into antioxidant and antimutagenic properties. *Journal of American Botanical Council*, 34-35.

Esfandiari N., Simchi A., & Bagheri R. (2013). Size tuning of Ag-decorated TiO2nanotube arrays for improved bactericidal capacity of orthopedic implants. *Journal of Biomedical Materials Research Part A, 102*(8), 2625-2635.

Evans P., & Sheel D. (2007). Photoactive and antibacterial TiO2 thin films on stainless steel. *Surface and Coatings Technology*, *201*(22-23), 9319-9324.

Feng Q.L., Wu J., Chen G.Q., Cui F.Z., Kim T.N., & Kim J.O. (2000). A mechanistic study of the antibacterial effect of silver ions on *Escherichia coli* and *Staphylococcus aureus*. *Journal of Biomedical Materials Research*, *52*(4), 662-668.

Fonyuy B.E. (2014). Prevalence of Water Borne Diseases within Households in the Bamendankwe Municipality-North West Cameroon. *Journal of Biosafety & Health Education*, *02*(03), 7.

Fordham W.R., Redmond S., Westerland A., Cortes E., Walker C., Gallagher C., Krchnavek R.R. (2014). Silver as a Bactericidal Coating for Biomedical Implants. *Surface and Coatings Technology*, *253*, 52-57.

Foster H.A., Ditta I.B., Varghese S., Steele A. (2011). Photocatalytic disinfection using Gamage J., & Zhang Z. (2010). Applications of Photocatalytic Disinfection. *International Journal of Photoenergy*, *2010*, 1-11.

Gamez G., Gardea-Torresdey J., Tiemann K., Parsons J., Dokken K., & Jose Yacaman M. (2003). Recovery of gold (III) by alfalfa biomass and binding characterization using X-ray microfluorescence. *Advances in Environmental Research, 7*(2), 563-571.

Gong D., Ho W.C., Tang Y., Tay Q., Lai Y., Highfield J.G., & Chen Z. (2012). Silver decorated titanate/titania nanostructures for efficient solar driven photocatalysis. *Journal of Solid State Chemistry*, 189, 117-122.

Gordon, M.H. (1990). The Mechanism of Antioxidant Action *in Vitro*. In: Hudson B.J.F. (eds) Food Antioxidants. Elsevier Applied Food Science Series. Springer, Dordrecht.

Guin D., Manorama S.V., Latha J.N., & Singh S. (2007). Photoreduction of silver on bare and colloidal TiO_2 nanoparticles/nanotubes: Synthesis, characterization, and tested for antibacterial outcome. *The Journal of Physical Chemistry C*, *111*(36), 13393-13397.

.

Hatchett D.W., & White H.S. (1996). Electrochemistry of Sulfur Adlayers on the Low-Index Faces of Silver. *The Journal of Physical Chemistry*, *100*(23), 9854-9859.

Henglein A., & Giersig M. (1999). Formation of Colloidal Silver Nanoparticles: Capping Action of Citrate. *The Journal of Physical Chemistry B*, *103*(44), 9533-9539.

Hossain F., Perales-Perez O.J., Hwang S., & Román F. (2014). Antimicrobial nanomaterials as water disinfectant: Applications, limitations and future perspectives. *Science of The Total Environment*, *466-467*, 1047-1059.

Hu C., Guo J., Qu J., & Hu X. (2007). Efficient destruction of bacteria with Ti (IV) and antibacterial ions in co-substituted hydroxyapatite films. *Applied Catalysis B: Environmental*, *73*(3-4), 345-353.

Igbeneghu O.A., & Lamikanra A. (2014). The bacteriological quality of different brands of bottled water available to consumers in Ile-Ife, south-western Nigeria. *BMC Research Notes*, *7*(1), 859.

Ikehata K., Gamal El-Din M., & Snyder S. A. (2008). Ozonation and Advanced Oxidation Treatment of Emerging Organic Pollutants in Water and Wastewater. *Ozone: Science & Engineering*, *30*(1), 21-26.

Jaya P.Y and Khushboo S. (2015). Past and present research systems of green chemistry. Organic Chemistry: *Current Research, 4*(2), 4172.

Joubert E. (1996). HPLC quantification of the dihydrochalcones, aspalathin and nothofagin in rooibos tea (*Aspalathus linearis*) as affected by processing. *Food Chemistry*, *55*(4), 403-411.

Joubert E., Gelderblom W., Louw A., & De Beer D. (2008). South African herbal teas: *Aspalathus linearis*, *Cyclopia spp*. and Athrixia phylicoides—A review. *Journal of Ethnopharmacology*, *119*(3), 376-412.

Jung W.K., Koo H.C., Kim K.W., Shin S., Kim S.H., & Park Y.H. (2008). Antibacterial Activity and Mechanism of Action of the Silver Ion in Staphylococcus aureus and Escherichia coli. *Applied and Environmental Microbiology*, *74*(7), 2171-2178.

Kaur K. & Komal R. (2016). Comparative analysis of antibacterial activity of Silver nanoparticles synthesized using leaf extract of wheat varieties. *International Journal of Nano Dimension*, *7*(2), 137–143.

Kedziora A., Strek W., Kepinski L., Bugla-Ploskonska G., & Doroszkiewicz W. (2012). Synthesis and antibacterial activity of novel titanium dioxide doped with silver. *Journal of Sol-Gel Science and Technology*, *62*(1), 79-86.

Khalil M.M., Ismail E.H., El-Baghdady K.Z., & Mohamed D. (2014). Green synthesis of silver nanoparticles using olive leaf extract and its antibacterial activity. *Arabian Journal of Chemistry*, *7*(6), 1131-1139.

Khatami M., Alijani H.Q., & Sharifi I. (2018). Biosynthesis of bimetallic and core–shell nanoparticles: their biomedical applications – a review. *IET Nanobiotechnology*, 8, 411.

Kim J., Lee S., Kim C., Seo J., Park Y., Kwon D., Choi K. (2014). Non-monotonic concentration–response relationship of TiO_2 nanoparticles in freshwater cladocerans under environmentally relevant UV-A light. *Ecotoxicology and Environmental Safety*, *101*, 240-247.

Kim S., Oh S., Lee S., & Choi S. (2008). Radiolytic synthesis of Pd-M (M=Ag, Ni, and Cu)/C catalyst and their use in Suzuki-type and Heck-type reaction. *Journal of Industrial and Engineering Chemistry*, *14*(4), 449-456.

Krishnamoorthy K., Manivannan G., Kim S.J., Jeyasubramanian K., & Premanathan M. (2012). Antibacterial activity of MgO nanoparticles based on lipid peroxidation by oxygen vacancy. *Journal of Nanoparticle Research*, *14*(9), 2-10.

Li Q., Mahendra S., Lyon D.Y., Brunet, L., Liga M. V., Li D., & Alvarez P.J. (2008). Antimicrobial nanomaterials for water disinfection and microbial control: Potential applications and implications. *Water Research*, *42*(18), 4591-4602.

Liu J. Zhimin W., Zhiping L., & Sajid B. (2013). Effective bactericidal performance of silver-decorated titania nano-composites. *Dalton Transactions*, (3), 2158–2166.

Liu C., Geng L., Yu Y., Zhang Y., Zhao B., & Zhao Q. (2018). Mechanisms of the enhanced antibacterial effect of Ag-TiO_2 coatings. *Biofouling*, *34*(2), 190-199.

Liu J., Wang Z., Luo Z., & Bashir, S. (2013). Effective bactericidal performance of silver-decorated titania nano-composites. *Dalton Trans*, *42*(6), 2158-2166.

Liu S., Wei L., Hao L., Fang N., Chang M.W., Xu, R., Chen Y. (2009). Sharper and Faster "Nano Darts" Kill More Bacteria: A Study of Antibacterial Activity of Individually Dispersed Pristine Single-Walled Carbon Nanotube. *ACS Nano*, *3*(12), 3891-3902.

Liu Y., Liu C., Rong Q., & Zhang Z. (2003). Characteristics of the silver-doped TiO_2 nanoparticles. *Applied Surface Science*, *220*(1-4), 7-11.

Loher S., Schneider O.D., Maienfisch T., Bokorny S., & Stark W.J. (2008). Micro-organism-Triggered Release of Silver Nanoparticles from Biodegradable Oxide Carriers Allows Preparation of Self-Sterilizing Polymer Surfaces. *Small*, *4*(6), 824-832.

Loo Y., Chieng B.W., Nishibuchi M., & Radu S. (2012). Synthesis of silver nanoparticles by using tea leaf extract from Camellia Sinensis, 7, 4263–4267.

Mah T.C., & O'Toole G.A. (2001). Mechanisms of biofilm resistance to antimicrobial agents. *Trends in Microbiology*, *9*(1), 34-39.

Martínez-Castañón G.A., Niño-Martínez N., Martínez-Gutierrez F., Martínez-Mendoza J.R., & Ruiz F. (2008). Synthesis and antibacterial activity of silver nanoparticles with different sizes. *Journal of Nanoparticle Research*, *10*(8), 1343-1348.

Matsunaga T. (1985). Photoelectrochemical sterilization of microbial cells by semiconductor powders. *FEMS Microbiology Letters*, *29*(1-2), 211-214.

Metzler A., & Huang D. (2015). Inhibition of bacteria by photocatalytic nano-TiO_2 particles in the absence of light. *International Journal of Environmental Science and Technology, 12*(9), 2987–2996.

Missengue R.N., Musyoka N.M., Madzivire G., Babajide O., Fatoba O.O., Tuffin M., & Petrik L.F. (2015). Leaching and antimicrobial properties of silver nanoparticles loaded onto natural zeolite clinoptilolite by ion exchange and wet impregnation. *Journal of Environmental Science and Health, Part A, 51*(2), 97-104.

Mohammed Fayaz A., Balaji K., Kalaichelvan P., & Venkatesan R. (2009). Fungal based synthesis of silver nanoparticles—An effect of temperature on the size of particles. *Colloids and Surfaces B: Biointerfaces*, *74*(1), 123-126.

Mohmood I., Lopes C. B., Lopes I., Ahmad I., Duarte A.C., & Pereira E. (2013). Nanoscale materials and their use in water contaminants removal—a review. *Environmental Science and Pollution Research*, *20*(3), 1239-1260.

Morones J.R., Elechiguerra, J.L., Camacho A., Holt K., Kouri J.B., Ramírez J.T., & Yacaman M.J. (2005). The bactericidal effect of silver nanoparticles. *Nanotechnology*, *16*(10), 2346-2353.

Motlagh Labbani A., Bastani S., & Hashemi M. (2014). Investigation of synergistic effect of nano sized Ag/TiO_2 particles on antibacterial, physical and mechanical properties of UV-curable clear coatings by experimental design. *Progress in Organic Coatings*, *77*(2), 502-511.

Muniandy S., Kausb N., Sasidharanc S. (2017). One-step green synthesis of TiO2-Ag nanocomposites and their performance towards photocatalytic activities and antimicrobial properties. *Malaysian Journal of Catalysis*, 2, 28–34.

Nainani R., Thakur P., & Chaskar M. (2012). Synthesis of silver doped TiO_2 nanoparticles for the improved photocatalytic degradation of methyl orange. *Journal of material science and engineering, 2*(1), 52–58.

Nakagawa Y., Wakuri S., Sakamoto K., Tanaka R. (1997). The photogenotoxicity of titanium dioxide particles. *Mutation Research*, 394, 125–132.

Nataro J., Kaper J. (1998). Diarrheagenic *Escherichia coli*. *Clinical Microbiology Reviews*, 11, 142–201.

Navarro E., Piccapietra F., Wagner B., Marconi F., Kaegi R., Odzak N., Behra R. (2008). Toxicity of Silver Nanoparticles to *Chlamydomonas reinhardtii*. *Environmental Science & Technology, 42*(23), 8959-8964.

Nigussie G.Y., Tesfamariam G.M., Tegegne B.M., Weldemichel Y.A., Gebreab T.W., Gebrehiwot D.G., & Gebremichel G.E. (2018). Antibacterial Activity of Ag-Doped TiO2 and Ag-Doped ZnO Nanoparticles. *International Journal of Photoenergy*, 1-7.

Nishibuchi M., Chieng Nishibuchi M., & Loo Y.Y. (2012). Synthesis of silver nanoparticles by using tea leaf extract from *Camellia Sinensis*. *International Journal of Nanomedicine*, 7, 4263-4267.

Nyamukamba P., Tichagwa L., & Greyling. (2012). The influence of carbon doping on TiO_2 nanoparticle size, surface area, anatase to rutile phase transformation and photocatalytic activity. *Materials Science Forum* 712, 49-63.

O'Connor DR. (2002). Report of the Walkerton Inquiry: The events of May 2000 and related issues. Part 1: A summary. Toronto, Ontario, Ontario Ministry of the Attorney General, Queen's Printer for Ontario

Ocsoy I., Temiz M., Celik C., Altinsoy B., Yilmaz V., Duman F. (2017). A green approach for formation of silver nanoparticles on magnetic graphene oxide and highly effective antimicrobial activity and reusability. *Journal of Molecular Liquids*, 227, 147–152.

Olaolu T., Akpor O., & Akor C. (2014). Pollution indicators and pathogenic microorganisms in wastewater treatment: Implication on receiving water bodies. *International Journal of Environmental Protection and Policy 2*(6), 205-212.

Pal A., Pehkonen S., Yu L., Ray M. (2007). Photocatalytic inactivation of gram-positive and gram-negative bacteria using fluorescent light. *Journal of Photochemistry and Photobiology A: Chemistry, 186*(2–3), 335–341.

Pal S., Tak Y.K., & Song J.M. (2007). Does the Antibacterial Activity of Silver Nanoparticles Depend on the Shape of the Nanoparticle? A Study of the Gram-Negative Bacterium Escherichia coli. *Applied and Environmental Microbiology, 73*(6), 1712-1720.

Panáček A., Kvítek L., Prucek R.., Kolář M., Večeřová R., Pizúrová N., Zbořil R. (2006). Silver colloid nanoparticles: Synthesis, characterization, and their antibacterial activity. *The Journal of Physical Chemistry B, 110*(33), 16248-16253.

Pandey P., Kass P., Soupir M., Biswas S., & Singh V. (2014). Contamination of water resources by pathogenic bacteria. *AMB Express, 4*(51), 1–16.

Pietta P. (2000). Flavonoids as Antioxidants. *Journal of Natural Products*, *63*(7), 1035-1042.

Prakash J., Kumar P., Harris R.A., Swart C., Neethling J.H., Van Vuuren A.J., & Swart H.C. (2016). Synthesis, characterization and multifunctional properties of plasmonic Ag–TiO_2 nanocomposites. *Nanotechnology*, *27*(35), 355707.

Pūle D. (2016). Conventional and alternative disinfection methods of legionella in water distribution systems – review. *Constructive science*, 19, 21–26.

Qu X., Alvarez P., & Li Q. (2013). Applications of nanotechnology in water and wastewater treatment. *Water Research*, *47*(12), 3931–3946.

Química D.D., Catalão R., & Goiás U.F.D. (2015). Dye degradation enhanced by coupling electrochemical process and heterogeneous photocatalysis. *Journal of the Brazilian Chemical Society*, *26*(9), 1817–1823.

Rai A., Singh A., Ahmad A., & Sastry M. (2006). Role of Halide ions and temperature on the morphology of biologically synthesized gold nanotriangles. *Langmuir*, *22*(2), 736-741.

Raimondi F., Scherer G.G., Kötz R., & Wokaun A. (2005). Nanoparticles in energy technology: Examples from electrochemistry and catalysis. *Angewandte Chemie International Edition*, *44*(15), 2190-2209.

Rao B., & Tang R. (2017). Green synthesis of silver nanoparticles with antibacterial activities using aqueous *Eriobotrya japonica* leaf extract. Advances in Natural Sciences: *Nanoscience and Nanotechnology*, 8, 015014.

Rasalingam S., Peng R., & Koodali R. (2014). Removal of hazardous pollutants from wastewaters: applications of TiO_2 –SiO_2 mixed oxide materials. *Journal of Nanomaterials*, 1-42.

Salkić A., & Ćavar Zeljković S. (2014). Preliminary investigation of bioactivity of Green tea (*Camellia Sinensis*), Rooibos (*Aspalatus Linearis*), and Yerba Mate (*Ilex Paraguariensis*). *Journal of Herbs, Spices & Medicinal Plants*, *21*(3), 259-266.

Sánchez-Valdes S., Ortega-Ortiz H., Ramos-de Valle L. F., Medellín-Rodríguez F. J., & Guedea-Miranda R. (2008). Mechanical and antimicrobial properties of multilayer films with a polyethylene/silver nanocomposite layer. *Journal of Applied Polymer Science*, 111, 953-962.

Sasi K R., Balasubramanian P., Govindaraj P., Krishnaveni T. (2014). Preliminary studies on phytochemicals and antimicrobial activity of solvent extracts of Coriandrum sativum L. roots (Coriander). *Journal of Pharmacognosy and Phytochemistry 2*(6): 74-78.

Saxena R., Sharma R., Nandy BC., & Jasuja ND. (2014) Qualitative and quantitative estimation of bioactive compounds in *Mimosa hamata*. *International Journal of Pharmacy and Pharmaceutical Sciences*, 6, 72-75.

Seery M., George R., & Floris, P. (2007). Silver doped titanium dioxide nanomaterials for enhanced visible light photocatalysis. *Journal of Photochemistry and Photobiology A*, 189 (2-3), 258-263.

Sezonov, G., Joseleau-Petit D., & D'Ari R. (2007). *Escherichia coli* Physiology in Luria-Bertani Broth. *Journal of Bacteriology*, *189*(23), 8746-8749.

Shaik M.R. Albalawi G, Khan S, Khan M, Adil S, Kuniyil M, Al-Warthan A, Siddiqui M, Alkhathlan H., & Khan M. (2016). "Miswak" based green synthesis of silver nanoparticles: evaluation and comparison of their microbicidal activities with the chemical synthesis. *Molecules*, 21, 1478.

Shannon M., Bohn P., Elimelech M., Georgiadis J., Marinas B., and Mayes A. (2008). Science and technology for water purification in the coming decades. *Nature,* 452, 301–310.

Sharma V., Yngard R., & Lin Y. (2009). Silver nanoparticles: Green synthesis and their antimicrobial activities. *Advances in Colloid and Interface Science, 145*(1–2), 83–96.

Shrivastava S., Bera T., Roy A., Singh G., Ramachandrarao P., & Dash D. (2007). Characterization of enhanced antibacterial effects of novel silver nanoparticles. *Nanotechnology*, *18*(22), 225103.

Simpson M., Hjelmqvist D., López-Alarcón C., Karamehmedovic N., Minehan T., Yepremyan A., Alarcon E. (2013). Anti-peroxyl radical quality and antibacterial properties of Rooibos infusions and their pure glycosylated polyphenolic constituents. *Molecules*, *18*(9), 11264-11280.

Sineiro J., Franco D., Rubilar M., Sánchez M, Jerez M, Pinelo M, Costoya N, JoséNúñez M. (2008). Polyphenols from plant materials: extraction and antioxidant power. Electronic *Journal of environmental, Agricultural and Food chemistry*, 7(8), 3210-3216.

Sithole N. (2015). Synthesis of silver nanoparticles and investigating their antimicrobial effects. Published master's thesis. *University of the Western Cape,* Bellville, South Africa.

Slavin Y.N., Asnis J., Häfeli O.U., Bach H. (2017). Metal nanoparticles: understanding the mechanisms behind antibacterial activity. *Journal of Nanobiotechnology,* 15, 65.

Sondi I., & Salopek-Sondi B. (2004). Silver nanoparticles as antimicrobial agent: a case study on *E. coli* as a model for Gram-negative bacteria. *Journal of Colloid and Interface Science*, *275*(1), 177-182.

Soni H., Ji Kumar., Patel K., & Kumar R. (2017). Metallic Nano-particles as alternative anti-microbial. *Journal of Nano-medicine Research*. 6(4), 00165.

Sulaiman G.M., mohammad A., Abdul-wahed H.E., Ismail M.M. (2013). Biosynthesis, antimicrobial and cytotoxic effects of silver nanoparticles using *Rosmarinus Officinalis* extract. *Digest Journal of Nanomaterials and Biostructures*. *8*(1), 273 - 280.

Tian L., Shen b., Xu H., Li F., Wang Y., Singh S. (2016). Thermal behavior of waste tea pyrolysis by TG-FTIR analysis. *Energy*, 103, 533-542.

Tortora G., R.B. Funke R.B., & Case L.C. (2001). Microbiology: An Introduction Addison-Wesley Longman Inc., New York.

Tyagi P.K., Singh R., Vats S., Kumar D., & Tyagi S. (2012). Nanomaterials use in wastewater treatment. *Nanotechnology and Chemical Engineering*, 21-22.

Ulicná O., Greksák M., Vancová O., Zlatos L., Galbavy S., Bozek P., Nakono M. (2003). Hepatoprotective effect of Rooibos tea (*Aspalathus linearis*) on CCl4-induced liver damage in rats. *Physiology Research* 52, 461-466.

United Nations, The report of the high-level panel of eminent persons on the post-2015 Development Agenda, UN, New York, 2013. Accessed, 30, May 2013.

Upadhyayula V., Deng S., Mitchell M., & Smith G. (2009). Application of carbon nanotube technology for removal of contaminants in drinking water: A review. *Science of the Total Environment, 408*(1), 1–13.

WHO, UNICEF. (2000). Global Water Supply and Sanitation Assessment Report. World Health Organization and United Children's Fund. http://www.who.int/docstore/water_sanitation_health/Globalassessment/GlobalTOC.htm

Wolfrum E.J., Huang J., Blake D.M., Maness P., Huang Z., Fiest J., & Jacoby W.A. (2002). Photocatalytic oxidation of bacteria, bacterial and fungal spores, and model biofilm components to Carbon Dioxide on Titanium Dioxide-coated surfaces. *Environmental Science & Technology*, *36*(15), 3412-3419.

Wong M., Chen C., Hsieh C., Hung S., Sun D., & Chang H. (2015). Antibacterial property of Ag nanoparticle-impregnated N-doped titania films under visible light. *Scientific Reports*, *5*(1),11978.

World Health Organization. (2014). Water Quality and Health. Drinking water chlorination – A review of disinfection practices and issues. http://www.waterandhealth.org/drinkingwater/wp.html. Accessed 28 Apr 2014.

Yu J., Xu D., Guan H.N., Wang C., Huang L.K., & Chi D.F. (2016). Facile one-step green synthesis of gold nanoparticles using Citrus maxima aqueous extracts and its catalytic activity. *Materials Letters*, 166, 110-112.

Zhang H., & Chen G. (2009). Potent Antibacterial Activities of Ag/TiO_2 nanocomposite powders synthesized by a One-Pot Sol−Gel method. *Environmental Science & Technology*, *43*(8), 2905-2910.

Zhang Q., Sun C., Zhao Y., Zhou S., Hu X., & Chen P. (2010). Low Ag-doped Titanium Dioxide nanosheet films with outstanding antimicrobial property. *Environmental Science & Technology*, *44*(21), 8270-8275.

Zhao Y., Sung W., Tsai T., & Wang H. (2010). Application of nanoscale Silver-doped Titanium Dioxide as photocatalyst for Indoor Airborne Bacteria Control: A feasibility study in medical nursing Institutions. *Journal of the Air & Waste Management Association*, *60*(3), 337-345.

Zhou K., & Yu L. (2004). Effects of extraction solvent on wheat bran antioxidant activity estimation. *LWT - Food Science and Technology*, *37*(7), 717-721.